Suid-Afrikaanse Tydskrif vir Natuurwetenskap en Tegnologie 2025; 44(1):33-52
South African Journal for Science and Technology 2025; 44(1):33-52
https://doi.org/10.36303/SATNT.2025.44.1.1021E

SATNT / SAJST
ISSN: 2222-4173 EISSN: 0254-3486

ORIGINAL RESEARCH

Homogeneous catalytic CO_2 capture by epoxides: kinetic-mechanistic study of corresponding cyclocarbonate formation

S Redgard, JA Venter, A Roodt

Department of Chemistry, University of the Free State, South Africa
Corresponding authors: *A Roodt, JA Venter* ***E-mail:*** *aroodta@gmail.com; venterja@ufs.ac.za*

The homogeneously catalysed CO_2 capture via cycloaddition to epichlorohydrin (EPI) as epoxide was studied via time-resolved ^{1}H NMR. It allowed an accurate and detailed *kinetic-mechanistic* analysis showing simple first-order kinetics with respect to EPI. It also provided significant insight into the reaction mechanism, which has not been studied previously in such depth. Several parameters were carefully evaluated, including a range of acids based on their Brønsted acidity, with ascorbic acid and benzoic acid selected as the target performers. The roles of TBAI (tetrabutylammonium iodide) and EPI were also systematically optimised, while the CO_2 concentration changes were evaluated under atmospheric pressure. The iodide ion was identified as the principal catalyst. The PGE complexes [Rh(COD)(L)Cl] (L = range of bases DBN, DBU, TMG), [Pd(COED)(N,N')]X (COED = η^3-6-methylcyclooct-2-en-1-id) and [Pt(COD)(N,N')Me]X (N,N'= range of bipyridine ligands), contrary to initial expectations, disappointingly indicated only slight activity. The results from the investigation led to the successful derivation of a proposed reaction scheme (both stoichiometric and catalytic) and rate law with four definite steps identified. It suggests that the ring opening of the epoxide is most probably the rate-determining step, yielding the expression (k_{obs}) for the disappearance of the epoxide, associated with an overall order of four.

Keywords: carbon dioxide; cyclocarbonate; homogeneous catalysis; kinetics; mechanism

Details regarding supplementary information are given at the end of this document.

Homogene katalitiese CO_2-vasvanging deur epoksiede: kineties-meganistiese studie van gepaardgaande siklokarbonaatvorming: Die homogeen-gekataliseerde CO_2-vasvanging via sikloaddisie deur epichloorhidrien (EPI) as epoksied is met behulp van tydgemoniteerde ^{1}H KMR bestudeer. Dit het 'n akkurate en gedetailleerde kineties-meganistiese analise moontlik gemaak en toon eenvoudige eersteordekinetika ten opsigte van EPI. Beduidende insig is verkry in die reaksiemeganisme, wat nie voorheen in soveel diepte bestudeer is nie. Verskeie parameters, met inbegrip van 'n reeks sure gebaseer op hul Brønsted-suursterkte, en met askorbien- en bensoësuur die gekose teikenpresteerders, is noukeurig geëvalueer. Die rol van die TBAI (tetrabutielammoniumjodied) en EPI is ook sistematies geoptimaliseer, terwyl die CO_2-konsentrasieverandering onder atmosferiese druk geëvalueer is. Die jodiedioon is as die hoofkatalisator geïdentifiseer. Die PGE-komplekse [Rh(COD)(L)Cl] (L = reeks basisse DBN, DBU, TMG), [Pd(COED)(N,N')]X (COED = η^3-6-metielsiklookt-2-een-1-ied) en [Pd(COD)(N,N')Me]X (N,N' = reeks bipiridienligande) was teleurstellend en het teenstrydig met aanvanklike verwagtings slegs geringe reaktiwiteit geïnduseer. Die resultate het gelei tot die suksesvolle daarstelling van 'n volledige reaksieskema (beide stoïgiometries en katalities) en 'n tempowet met vier definitiewe stappe wat geïdentifiseer is. Dit dui daarop dat die ringopening van die epoksied heelwaarskynlik die tempobepalende stap is, wat die uitdrukking vir die waargenome tempokonstante (k_{wg}) vir die verdwyning van die epoksied lewer, geassosieer met 'n algehele reaksieorde van 4.

Sleutelwoorde: koolstofdioksied; siklokarbonaat; homogene katalise; kinetika; meganisme

Besonderhede aangaande aanvullende inligting vir hierdie artikel word aan die einde van hierdie dokument gegee.

Introduction

The pollutant at the forefront of the greenhouse gases (GHGs) is carbon dioxide (CO_2), which is the leading contributor (74,4%) to global warming. The global emissions of CO_2 from fossil fuels were at record levels in 2019 (36,6 $GtCO_2$ – down to 34 $GtCO_2$ in 2020), with the largest emitters being China and the United States of America (USA) with 10,37 and 4,71 billion tonnes, respectively, in 2020 (NOAA-Global-Monitoring-Laboratory-US-Department-of-Commerce, 2021) (Le Quéré et al., 2021). The main drivers for CO_2 emissions from fossil fuels based on 2016 data, were heat and electricity generation (42%) (Ritchie & Roser, 2021). Additionally, China accounted for a staggering 25% of global energy consumption (58% from coal) in 2019 (O'Meara, 2020). Currently, 27 countries (including South Africa) have implemented some form of carbon taxation to reduce their national emissions, with some 31 countries and the European Union going a step further by setting greenhouse gas (GHG) neutrality dates, aiming to achieve it by 2060 (Earth.Org, 2021) (Advani, Prinz, Smurra, & Warwick, 2021) (ClimateAction-Tracker, 2021) (Kim et al., 2020) (Lamb et al., 2021).

Land and ocean sinks remove approximately 56% of global anthropogenic CO_2 emissions every year, with the remainder left in the atmosphere (Blunden & Boyer, 2021) (Masson-Delmotte, et al., 2021). Therefore, mitigation strategies are required to complement nature's efforts by reducing or removing pollutant emissions in the form of renewable energy sources or negative emission technologies (NETs) (Fawzy et al., 2020). In this regard, nature holds the secret to overcoming this problem via photosynthesis, using the best example of an NET that uses direct air capturing to eventually produce glucose.

However, plants have different mechanisms that are generally specific to a plant *genus* and are classified as C_3, C_4 and CAM (crassulacean acid metabolism) (Schlüter & Weber, 2020) (Berardi et al., 2014) (Bar-Even et al., 2010). The core mechanism of transforming CO_2, eventually into glucose is defined by the Calvin cycle, which is catalysed by the ribulose-1,5-bisphosphate carboxylase/oxygenase (RuBisCO) enzyme and is present in all three of the mechanisms. The C_4 (and CAM) mechanism have the benefit of an extra enzyme (phosphoenolpyruvate carboxylase (PEPc)) that fixes CO_2 to pyruvate to form a 4-carbon molecule, such as malic or oxalic acid (Schlüter & Weber, 2020) (Weber & Bar-Even, 2019). Research into optimising and/or rewiring the mechanisms within plants led to a new-to-nature carboxylation enzyme, glycolyl-CoA carboxylase (GCC). It was developed from the hypothetical tartonyl-CoA (TaCo) pathway which directly assimilates glycolate into C_3 metabolites by fixing CO_2 instead of releasing it. It showed comparable turnover numbers (TON = 1,4-11,1 s^{-1}) to natural enzymes (average TON = 10 s^{-1}) and most RuBisCOs (TON = 1-10 s^{-1}) (Trudeau et al., 2018) (Scheffen et al., 2021).

NETs incorporate a range of possibilities such as direct air capturing that can then use the captured CO_2 as a C_1-feedstock to synthesis other products. These include cyclocarbonates and polycarbonates with an epoxide as the substrate (Guil-López et al., 2019). Cyclocarbonates have a range of applications such as in polymer synthesis, lithium-ion battery electrolytes and dipolar aprotic solvents (Guo et al., 2021) (Jessop 2011) (Bello Forero et al., 2016) (Schäffner et al., 2008) (Schäffner et al., 2008) (Berh et al., 2002) (Lenden et al., 2011). Thus, in spite of the fact that CO_2 is relatively unreactive (linear non-polar molecule), requiring significant energy inputs to be transformed (ΔG_f° = -394 $kJmol^{-1}$) (Aresta & van Eldik, 2014), this route provides a solution to at least remove a (small) part of the CO_2 via a workable NET.

Primary chemical products industrially synthesised from CO_2 are listed in Table S1 (Guil-López et al., 2019). The use of epoxides as substrates to capture CO_2 (via late transition metal catalysts, including platinum group metals) produces cyclocarbonates as 'green' solvents (Alder et al., 2016) (Paddock & Nguyen, 2004) (Ramidi et al., 2013) (Khoshro et al., 2013) (Wang et al., 2012). These catalysts are effective in the exothermic process of CO_2 cyclo addition, see Fig. S15 (North & Styring, 2019) (Lamb 2019) (Büttner, et al., 2017).

Potential pathways for CO_2 fixation may be summarised under three key topics

i. In organic and organometallic systems CO_2 acts as a Lewis acid in the presence of a Lewis or Brønsted base, and can be captured by various classes of organic bases (for example amidines and guanidines) (Sopeña, et al., 2018) (Heldebrant et al., 2005).
ii. More bulky (stericallly demanding) bases with these functional groups have been able to capture CO_2 from ambient air (Seipp et al., 2017).
iii. Organometallic systems (including late transition metals and PGEs) (Paddock & Nguyen, 2004) (Ramidi et al., 2013) (Khoshro et al., 2013) (Wang, et al., 2012), which catalyse CO_2 reactions, are known (Pradhan & Das, 2023) (Schilling & Das, 2020) (Cauwenbergh et al., 2022) (Vermaak et al., 2024). This research shows promising results also with regard to electrocatalysis (Wu et al., 2019) (Khoshro et al., 2013) and photocatalysis (Kuehnel et al., 2017) (Nakada et al., 2015).

Relevant PGE systems include complexes containing 1,5-cyclooctadiene (COD), as a neutral bidentate ligand (Hill, 2011) (Hill & Roodt, 2018) (Hill et al., 2013). The rhodium catalysts are used for hydrogenation of double bonds (Flörke et al., 1992) (Jiang et al., 2022) and related kinetic investigations of the substitution of the nucleophilic ligands (amidines and guanidines) by pyridine analogues (DMAP dimethylpyridine) showed a ten-fold increase in the forward rate constant in favour of the guanidine ligand (Redgard, 2019). Interestingly, the COD ligand can also undergo oxidation (De Bruin et al., 1999), as illustrated previously (Klein et al., 2015) (Klein et al., 1999).

The research presented in this article focuses directly on the potential use of epoxides as substrates to capture CO_2 via cyclocarbonate formation. It evaluates the homogeneous catalysis via organometallic (Watt et al., 2021) (Lee et al., 2017) (Dolai et al, 2020) and organic systems (Arayachukiat, et al., 2017) (Yingcharoen et al., 2019). Moreover, it reports a detailed and systematic kinetic-mechanistic study of the cyclocarbonate

formation from epoxides and CO_2. A range of different parameters which influences the process is carefully evaluated, enabling a complete rate law which also explains the catalytic process. A special focus was the type of Lewis acid, *i.e.*, an inorganic or metal catalyst, or an organic acid. The detailed mechanism of cyclocarbonate formation from epoxides and CO_2 and is thus presented as a potential workable option to generate a value added product (North & Styring, 2019).

Results and discussion

Evaluation of different parameters influencing the system

To systematically evaluate the system, several parameters were identified and considered to study the simplified reaction as indicated in Scheme 1.

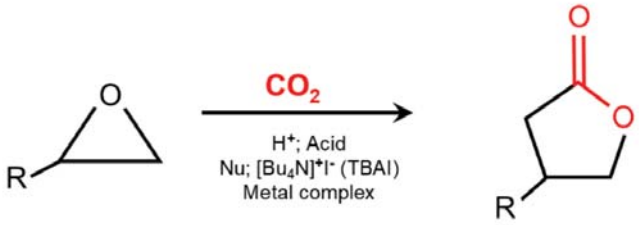

Scheme 1: Condensed representation of the current study. For structures of different epoxides see Fig. 1.

Firstly, a range of epoxides were selected based on literature followed by a systematic number of acids to confirm/contradict claims made in literature with respect to ascorbic acid in particular (Dolai et al., 2020) (Arayachukiat et al., 2017) (Yingcharoen et al., 2019). Next, different parameters, *i.e.*, the influence of tetrabutylammonium iodide (TBAI), selected acids and EPI were optimised. Finally, a number of metal catalyst models were evaluated under selected ambient conditions.

An illustration and discussion for all the reactions as monitored stepwise via ^{1}H-NMR are discussed in the different sub-sections below. For all these parameter variations, the turn-over-number [TON= (mol product)/(mol catalyst) after 23h] and the turn-over-frequency (TOF=TON/23 h), evaluated over the periods studied as indicated below, are also reported.

Selection of the epoxide

Four epoxides were evaluated (Fig. 1) which were epichlorohydrin (EPI), styrene oxide, cyclohexene oxide and limonene oxide. The epoxides chosen were to determine which one would best serve as a model epoxide for the CO_2 capturing reaction in terms of formation rate and distinguishable ^{1}H-NMR spectra of the product (see Fig. 2). Reactant and TBAI peaks based on previous literature work were also selected with increasing bulkiness (steric hindrance) (Fig.1(a)-(d)) to determine if it plays a role, and if so, to what extent (Dolai et al., 2020) (Arayachukiat et al., 2017) (Yingcharoen et al., 2019).

The product formation peaks, as shown in the ^{1}H-NMR stacked spectra (Fig. S18), were only observed for EPI (Fig. S18(a)) and styrene oxide (Fig. S18(b)), with the latter epoxide forming significantly slower than the EPI. Moreover, the stacked spectra of limonene- and cyclohexene oxide (Fig. S18(c), (d)) did not definitively show product formation and the peaks overlapped with the TBAI peaks, which increased the complexity of the system. Additionally, the latter two epoxides formed cyclocarbonate precipitates whereas EPI and styrene oxide remained liquids. Based on these results, it was concluded that epichlorohydrin (EPI) was the ideal model epoxide to further evaluate the process.

Preliminary NMR evaluation of product formation

The work by Dolai et al. (Dolai et al., 2020) was evaluated and extended to that of D'Elia (Arayachukiat et al., 2017) (Yingcharoen et al., 2019). Thus, with EPI selected, the actual carbon dioxide capture was evaluated in detail and as a function of time, see Figure 2.

To assess the reactions from a kinetic perspective, the reaction mixtures were dissolved in chloroform and an aliquot of the sample was periodically characterised by ^{1}H NMR spectroscopy. Upon further inspection of the spectra it was observed that a larger amount of the reactant had "disappeared" than the amount of product that had formed. Upon changing the solvent to benzene and acetone, the difference in the change of reactant and product was reduced. Literature suggested the cause was the possible decomposition of EPI to the highly toxic phosgene and carbon monoxide (CO) gases, which would account for them not being observed in the ^{1}H NMR spectra. IR spectroscopy was ruled out as a method to characterise the gases because of the overlapping peaks with chloroform and EPI. Instead, a carbon monoxide gas detector was used and confirmed the presence of CO.

Considering the above, it was therefore decided to use the epoxide as *neat* samples, so the use of a solvent in the reaction mixture was excluded. This was done not only for safety concerns but also because it led to a significant increase in the reaction time to achieve similar results to the solvent free reaction.

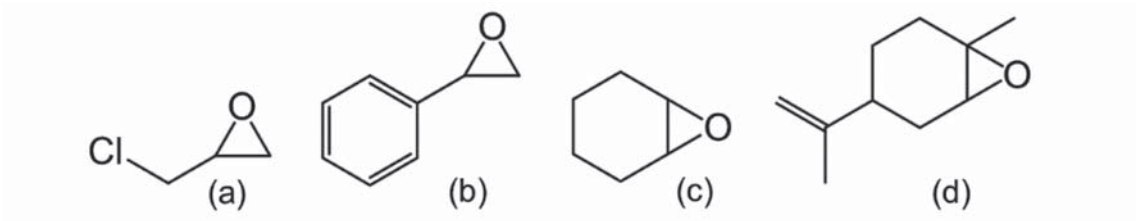

Figure 1: Structural illustration of the epoxides evaluated. (a) Epichlorohydrin (EPI), (b) styrene oxide, (c) cyclohexene oxide and (d) limonene oxide

Kinetic monitoring of the CO_2-insertion

Different parameters influence the process which are systematically discussed below. For example, acid addition to the system significantly activates the reaction. While the evaluation of the different acids are still to be discussed in more detail, Figure 3 visually illustrates the influence of the addition of an acid compared to its absence in a typical reaction. The other reaction conditions were identical (25 mmol EPI and 2 mmol TBAI) apart from 1 mmol benzoic acid addition for the reaction progression as shown.

It is therefore clear that the reactant(s) and product(s) in the insertion reaction are easily identified by ^{1}H NMR. Although it is quite expensive, ^{1}H NMR were thus used to kinetically monitor the reaction progress. This is typically illustrated in Figure 4 wherein the reactions clearly display simple first-order behaviour as defined by Equations (Eqs.) 13 and 14.

Variation of acids

Following the selection of an appropriate epoxide model, *i.e.*, EPI, a range of acids (Fig. 5) was evaluated to assess possible influences on the rate and formation of the EPcy from EPI. The acids which were selected are based on literature (ascorbic acid and benzoic acid) (Arayachukiat et al., 2017) (Yingcharoen et al., 2019). In addition succinic acid, tartaric acid and citric acid were selected, assuming that weaker acids are required to maintain/buffer the pH at mild acidic conditions, and ensuring that the CO_2 are well below the pK_a value of bicarbonate formation (Krieg et al., 2015). In addition to these acids, the reaction was also evaluated without the presence of an acid (control) and with a base (metformin) (Moghimi et al., 2011). The reaction conditions chosen were 23 mmol EPI, 1 mmol TBAI and 0,5 mmol acid with a CO_2 balloon setup (1 atm; see Fig. S16).

The results for the control, ascorbic acid and benzoic acid are presented in Table 1 and S2 (illustrated in Fig. 6) and the rest (metformin, succinic acid, tartaric acid and citric acid) in Table 1 and S3 (illustrated in Fig. 6a1 and a2). The observed rate constant (k_{obs}) for the EPcy formation and EPI consumption are shown along with the percentage of conversion to the product.

The presence of an acid clearly promotes the reaction when comparing to the control reaction, which only converted 13,1%. The ascorbic (38,5%) and benzoic (31,5%) acids had the highest conversion percentage of all the acids, followed by succinic

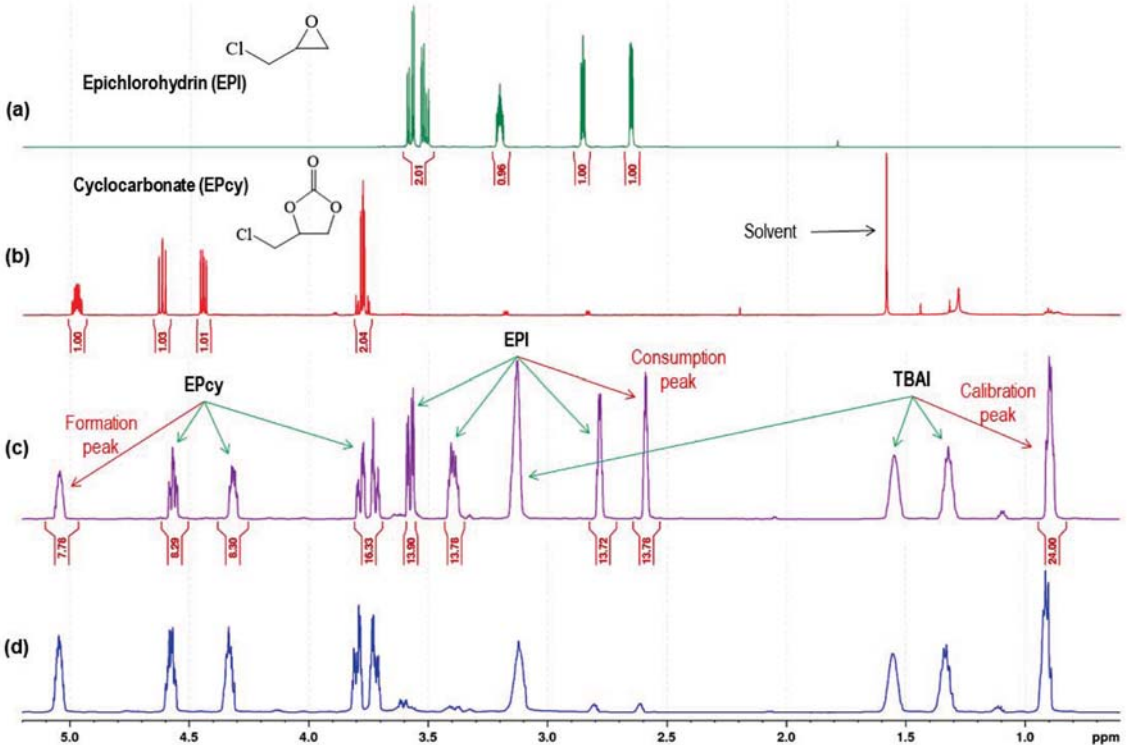

Figure 2: ^{1}H-NMR spectra of reactants and products as studied kinetically: (a) The ^{1}H-NMR spectrum of epichlorohydrin (EPI, reactant), (b) The ^{1}H-NMR spectrum of the cleaned (EPcy, product) with the residual solvent peak (H_2O), (c) The ^{1}H-NMR spectrum illustrating the peaks of the product (EPcy), reactant (EPI) and catalyst (TBAI) and (d) The reaction mixture when the product is not cleaned (contains TBAI). The red arrows in (c) indicate the peaks used to quantitatively measure the respective product formation quantities (EPcy) and reactant consumption quantities (EPI), as calibrated to the tetrabutylammonium cation (from accurately weighed amounts of TBAI) methyl protons.

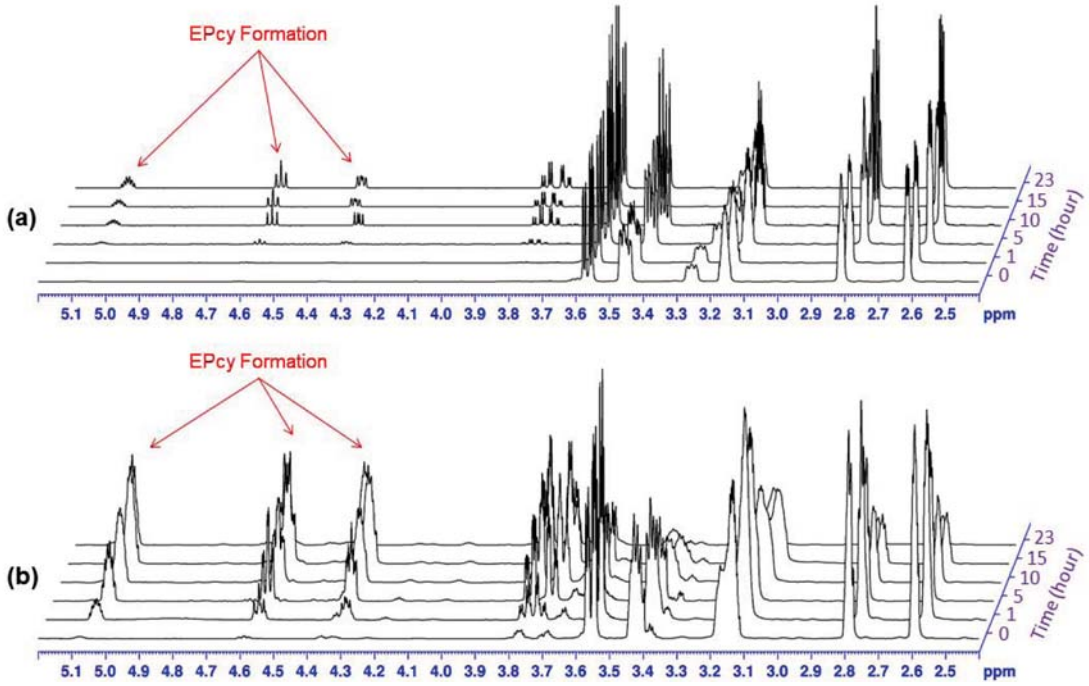

Figure 3: Stacked ^{1}H-NMR spectra of the reaction progression indicating cyclocarbonate (EPcy) formation at 0, 1, 5, 10, 15 and 23 hours from CO_2 trapping by EPI with (a) TBAI and (b) TBAI and benzoic acid. Reaction conditions: 25 mmol EPI, 2mmol TBAI, [CO_2] = 1 atm. 25 mmol EPI, 2 mmol TBAI, [CO_2] = 1 atm, at room temperature (1 mmol benzoic acid mmol for (b) only).

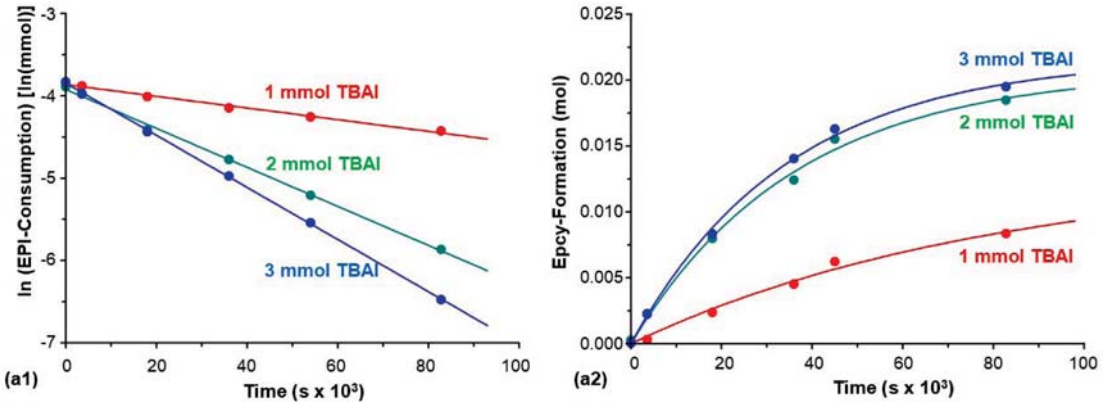

Figure 4: Illustration of the (a) epichlorohydrin (EPI) first order consumption (L.S. fit to Equation (Eq.) 14) and (b) cyclocarbonate (EPcy) formation [L.S. fit to Eq. 13], confirming the first-order dependence on both the EPI and the EPcy (Table S4). Reactions are at different TBAI concentrations as indicated, using ascorbic acid and CO_2 (1 atm; via balloon setup, see also Fig. S16) at room temperature. [EPI] = 22 mmol, [CO_2] = 1 atm, [TBAI] = 1,2,3 mmol, [acid] = 0,5 mmol.

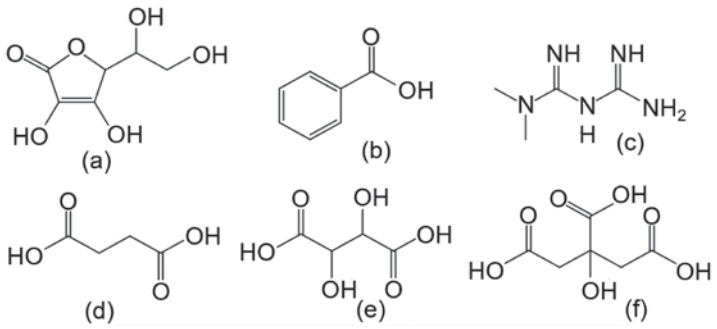

Figure 5: Graphical representation of acids and the base assessed: (a) ascorbic acid, (b) benzoic acid, (c) metformin, (d) succinic acid, (e) tartaric acid and (f) citric acid.

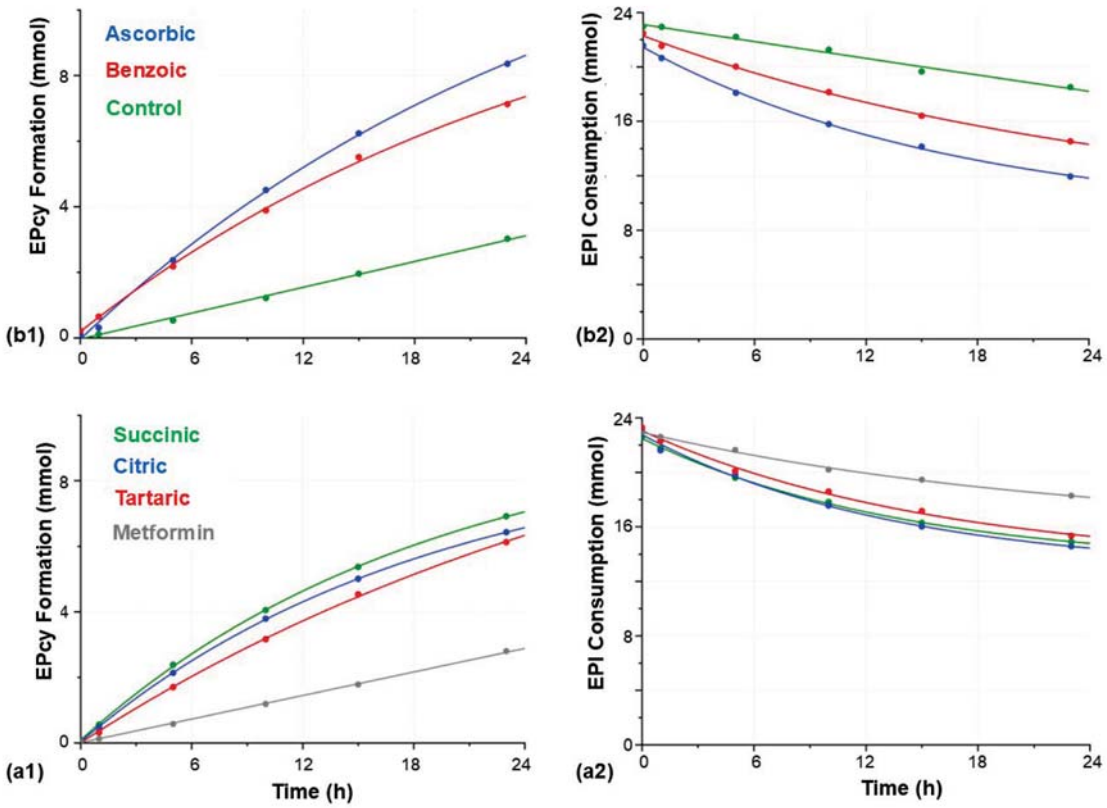

Figure 6: Illustration of the L.S. fits (Eq. 13) of the (a) EPcy formation [a1 and b1] and (b) EPI consumption [a2 and b2]. Reactions are in the presence of different acids, TBAI and CO_2 at room temperature. [EPI] = 23 mmol, [CO_2] = 1 atm, [TBAI] = 1 mmol, [acid] = 0,5 mmol, (Table S2 and Table S3).

(30,5%), citric (27,8%) and tartaric acid (26,3%), see Table S2 and S3. The presence of metformin inhibited the reaction and resulted in a smaller conversion (12,2%) than the control. Consequently, the turnover number (TON), with respect to TBAI, followed the same trend with ascorbic acid being the highest (8,4) and metformin the lowest (2,8).

While ascorbic and benzoic acid had the highest conversion, succinic and citric acid had significantly higher observed rate constants (k_{obs}) of (15 ± 1) x $10^{-6}s^{-1}$ whereas the rates for ascorbic and benzoic acid were (10 ± 2) x $10^{-6}s^{-1}$ and (10 ± 1) x $10^{-6}s^{-1}$, respectively. Based on the results, ascorbic and benzoic acid were chosen as they resulted in the largest conversions. Additionally, the two acids were used to evaluate the other parameters to determine if they showed the same behaviour or differed: succinic, citric, tartaric acid and a base (metformin). The latter showed virtually the same conversion activity as the blank run.

TBAI-optimisation

Two acids (ascorbic and benzoic acid) were therefore chosen to further evaluate the optimal concentration of TBAI for the associated acid. The reaction conditions were 1, 2 and 3 mmol TBAI, 22 mmol EPI, and 0,5 mmol acid with a CO_2 balloon setup (1 atm, illustrated in Fig. S16). Additional TBAI concentrations were assessed (1,25, 1,50 and 1,75 mmol) with benzoic acid to evaluate the exponential increase in the reaction between 1 and 2 mmol TBAI.

Very importantly, it was noted that the reaction did not occur in the absence of TBAI.

The results for the ascorbic acid associated reactions are shown in Table S4 (illustrated in Fig. 7b) and benzoic acid associated reactions are shown in Table S5 (illustrated in Fig. 7a). The observed rate constant (k_{obs}) for the formation and consumption are shown along with the percentage of conversion to the product, TON and TOF. Both acids showed significantly improved conversions at higher TBAI concentrations of 2 mmol and 3 mmol when compared to 1 mmol. Ascorbic showed the largest conversion of 89,4% with 2 mmol TBAI compared to the 71,7% for benzoic acid. The turnover number (TON), in terms of TBAI, was also the highest at 2 mmol for both acids, with the ascorbic acid reaction (9,2) showing a higher value than the benzoic acid reaction (8,0). However, the observed rate constants of the ascorbic acid reaction (k_{obs} = (25 ± 1) x $10^{-6}s^{-1}$) were slightly lower than the benzoic acid reaction (k_{obs} = (28 ± 3) x$10^{-6}s^{-1}$).

The stepwise increase in the conversion percentage and the k_{obs} value that was observed between 1 and 2 mmol TBAI for both acids (Table S4, S5) was further assessed with benzoic acid. The reaction conditions were repeated for 1,25, 1,50 and 1,75 mmol TBAI to better understand the increase in the values (Table S5, Fig. 8).

The results showed an increasing trend between the three TBAI concentrations for the k_{obs} and the conversion percentage.

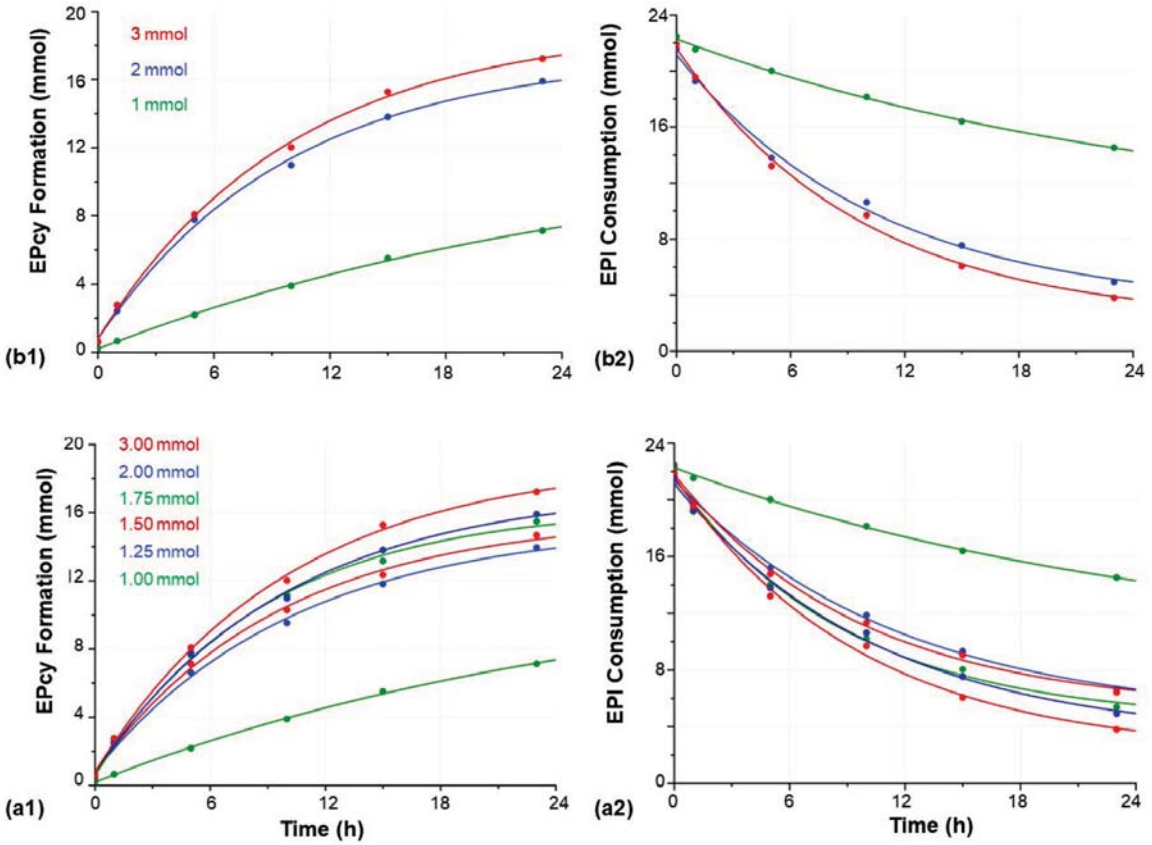

Figure 7: Illustration of the L.S. fits (Eq. 13) in the presence of (a) benzoic acid [a1 and a2] (Table S5) and (b) ascorbic acid [b1 and b2] (Table S4) as illustrated in the of EPcy formation and EPI consumption. Reactions are at different TBAI concentrations, and CO_2 at room temperature. [EPI] = 22 mmol, [CO_2] = 1 atm, [acid] = 0,5 mmol, [TBAI] = 1,00, 1,25, 1,50, 1,75, 2,00 and 3,00 mmol. See also Figure 11(b).

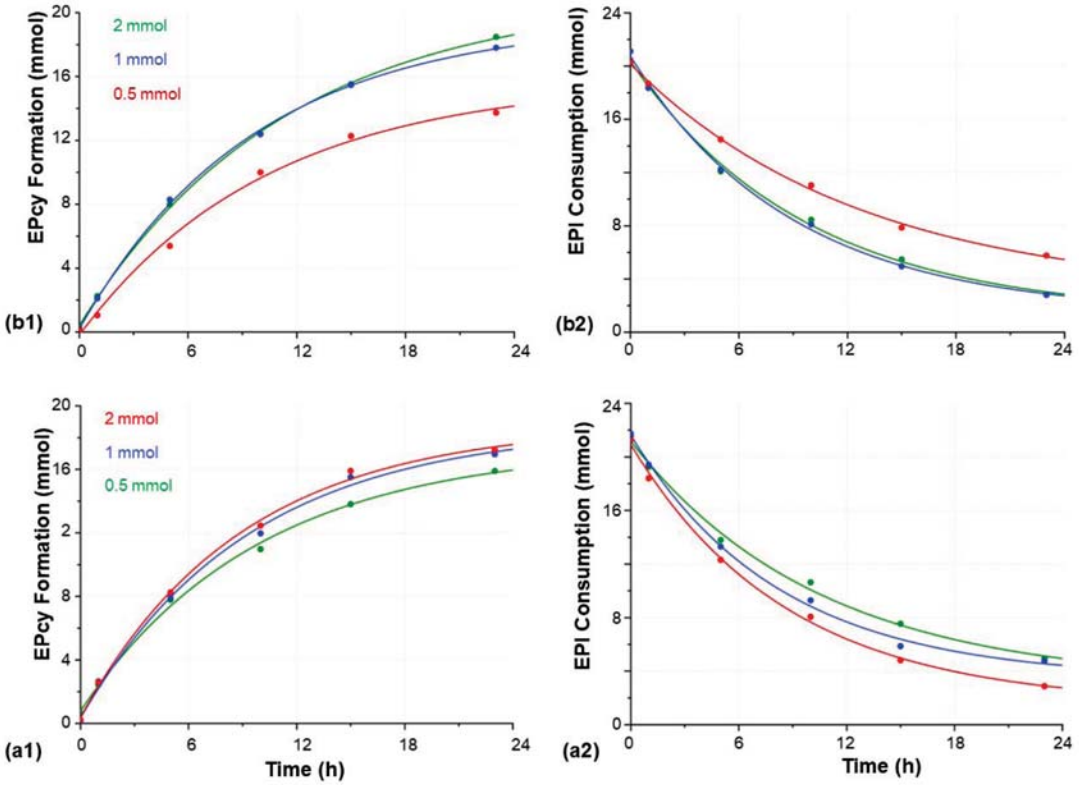

Figure 8: Illustration of the L.S. fits (Eq. 13) of (a) EPcy formation [a1 and b1] and (b) EPI consumption [a2 and b2]. Reactions are at (a) different ascorbic acid concentrations, (Table S6) (b) different benzoic acid concentrations, (Table S7), see also Figure 11(b). Room temperature. [EPI] = 22 mmol, [CO_2] = 1 atm, [TBAI] = 2 mmol, [acid] = 0,5, 1, 2 mmol.

However, when the k_{obs} of the all the TBAI concentrations were compared to each other (Fig. 7) the relationship suggested a stepwise increase which reaches equilibrium/'saturation' at 1,50 mmol TBAI {equilibrium evidenced. See also Fig. 11(b)}. Considering all the results with 2 mmol TBAI, further experiments were continued with this amount.

Acid optimisation

The next step was to determine the optimal concentration of the two acids (ascorbic and benzoic acid). The reaction conditions were 2 mmol TBAI, 22 mmol EPI, and 0,5, 1 and 2 mmol acid with a CO_2 balloon setup (1 atm). The results for the ascorbic acid associated reactions are shown in Table S6 (illustrated in Fig. 8a) and benzoic acid in Table S7 (illustrated in Fig. 8b). The observed rate constant (k_{obs}) for the formation and consumption are shown along with the percentage of conversion to the product, TON and TOF.

The behaviour of both acids differed significantly from one another, showing an increase in conversion with an increase in the acid. The ascorbic acid conversions were the highest at 0,5 mmol (89,4%) and lowest at 2 mmol (67,3%), whereas the benzoic acid conversions were the highest at 2 mmol (80,1%) and lowest at 0,5 mmol (71,7%). However, both acids had comparable observed rate constants (k_{obs}) at 1 mmol, with the ascorbic acid being $(29 \pm 2) \times 10^{-6} s^{-1}$ and the benzoic acid reaction being $(30 \pm 4) \times 10^{-6} s^{-1}$.

To maintain comparable reaction results between the acids, 1 mmol acid was selected as the optimised concentration to continue further. Moreover, benzoic acid (HBz) was also selected because there is a clearer independence of [HBz] across the concentration range studied.

Epoxide optimisation

The concentration of the epoxide was evaluated next to determine the best concentration to follow the reaction for ca. 24 hours. The three concentrations of EPI were approximately 25, 40 and 55 mmol (values differed between respective acid reactions based on the calibration peak (TBAI). The other reaction conditions were kept constant, *i.e.*, 2 mmol TBAI and 1 mmol acid with a CO_2 balloon setup (1 atm). The results for the ascorbic acid associated reactions are shown in Table S8 (illustrated in Fig. S17a) and benzoic acid associated reactions are shown in Table S9 (illustrated in Fig. S17b). The observed rate constant (k_{obs}) for the formation and consumption are shown along with the percentage of conversion to the product, TON and TOF.

Both acids showed similar trends for the conversion percentage and k_{obs} of decreasing values with an increase in the EPI concentrations. The ascorbic acid conversions were the highest at 21 mmol EPI (83,9%) and lowest at 45 mmol EPI (64,4%), while the benzoic acid conversions were the highest at 22 mmol EPI (77,9%) and lowest at 50 mmol EPI (54,4%). The observed rate constants (k_{obs}) of the acids were the highest at the lowest EPI concentrations with values of $(29 \pm 2) \times 10^{-6} s^{-1}$ for the ascorbic acid and $(30 \pm 4) \times 10^{-6} s^{-1}$ for benzoic acid.

However, the decrease in the k_{obs} values was concluded to be simply due to the *dilution* of the other reactants (TBAI, CO_2 and the acid), i.e. from 21 to 33 to 45 mmol, which display k_{obs} values for the product formation of $(29 \pm 2) \times 10^{-6} s^{-1}$, $(15 \pm 2) \times 10^{-6} s^{-1}$ and $(12 \pm 1) \times 10^{-6} s^{-1}$ (ascorbic acid, see Table S6), and $(30 \pm 4) \times 10^{-6} s^{-1}$, $(17 \pm 3) \times 10^{-6} s^{-1}$ and $(15 \pm 3) \times 10^{-6} s^{-1}$ (benzoic acid), for 22, 35 and 50 mmol EPI, respectively, see Table S7. Clearly, the dilution played an important part in this.

In fact, these values, when they are normalised relative to 25 mmol, essentially give identical k_{obs} values: $(24 \pm 2) \times 10^{-6} s^{-1}$, $(20 \pm 3) \times 10^{-6} s^{-1}$ and $(22 \pm 2) \times 10^{-6} s^{-1}$ (for ascorbic acid), and $(26 \pm 4) \times 10^{-6} s^{-1}$, $(24 \pm 4) \times 10^{-6} s^{-1}$ and $(30 \pm 6) \times 10^{-6} s^{-1}$ (for benzoic acid), respectively in increased order of their EPI-concentrations. It confirms that (a) the rate constants are the same within estimated standard deviations (estimated standard deviation), and (b) the first order dependence (again) of the rate constants on [EPI] as reactant, as shown above.

Since the highest conversions were achieved with the lower EPI concentrations, they were chosen since it allowed for a better least-squares fitting of the data to determine the k_{obs}. Additionally, benzoic acid was selected as the acid because of structural simplicity when compared to ascorbic acid (Figure 5).

Metal complex evaluation

Two metal catalysts, [Rh(COD)(DBN)Cl] (1,5-diazabicyclo[4.3.0] non-5-ene (DBN)) and [Pd(COED)-(DiOMeBpy)]BF_4 (Pd-1) were evaluated next to determine the best concentration to follow the reaction for 23 hours. The three concentrations of the metals were approximately 0,025, 0,050 and 0,100 mmol. The reaction conditions were 2 mmol TBAI and 1 mmol benzoic acid with the CO_2 balloon setup (1 atm). The results for the [Rh(COD)(DBN)Cl] associated reactions are shown in Table S10 and [Pd(COED) (DiOMeBpy)]BF_4 shown in Table S11 (both illustrated in Fig. 9). The observed rate constant (k_{obs}) for the formation and consumption are shown along with the percentage of conversion to the product, TON and TOF.

The [Rh(COD)(DBN)Cl] catalyst was compared to [Rh(COD)(DBU) Cl] and [Rh(COD)(TMG)Cl] {1,8-diazabicyclo[5.4.0]undec-7-ene (DBU) and 1,1,3,3-tetramethyl guanidine (TMG)}. The results for the rhodium complexes associated reactions are shown in Table S12 (illustrated in Fig. 9a). On the other hand, the [Pd(COED) (DiOMeBpy)]BF_4 (**Pd-1**) catalyst was compared to [Pd(COED) (Bpy)]SbF_6 (**Pd-2**), Table S13 (Fig. 9b). The [Rh(COD)(L)Cl] complexes (**DBN**, **DBU** and **TMG**) only differed in their ligand and showed different results for all their values. The conversion percentage decreased in order of the ligands DBN (78,7%), DBU (74,8%) and TMG (71,9%), and the observed rate constant (k_{obs}) was the same for DBN $\{(30 \pm 2) \times 10^{-6} s^{-1}\}$ and DBU $((30 \pm 3) \times 10^{-6} s^{-1})$ while TMG $((32 \pm 3) \times 10^{-6} s^{-1})$ was marginally larger.

The conversion percentage and the k_{obs} of [Pd(COED)(DiOMeBpy)]BF_4 (Pd-1) and [Pd(COED)(Bpy)]SbF_6 (Pd-2) differed significantly from one other. The conversion for Pd-1 was 77,2% and 72,3% for Pd-2 while their respective k_{obs} values were (29 ± 5) x $10^{-6}s^{-1}$ and (25 ± 2) x $10^{-6}s^{-1}$.

The conversion and observed rate constant (k_{obs}) for the rhodium complex was slightly higher at all concentrations when compared to the palladium complex. Interestingly, the complexes showed a small tendency (although not significant) of an inverse relationship with their conversions. For [Rh(COD)(DBN)Cl] the conversion increased to 79,7% (0,050 mmol), from 78,7% (0,025 mmol), then decreased to 77,7% (0,100 mmol), where [Pd(COED)(DiOMeBpy)]BF_4 decreased from 77,2% (0,025 mmol) to 75,0% (0,050 mmol) then increased to 75,6% (0,100 mmol).

The conversion trend for [Pd(COED)(DiOMeBpy)]BF_4 was the same for its observed rate constant while the k_{obs} for [Rh(COD)(DBN)Cl] was identical at concentrations of 0,025 mmol {(30 ± 2) x $10^{-6}s^{-1}$} and 0,050 mmol and {(30 ± 3) x $10^{-6}s^{-1}$}, and higher at 0,100 mmol {(33 ± 4) x $10^{-6}s^{-1}$}. The highest TON for both complexes were at 0,050 mmol (TON = 8,8) for the rhodium complex and at 0,025 mmol (TON = 8,5) for the palladium complex.

The lower concentration (0,025 mmol) was next used to evaluate other complexes for a comparative analysis. The fact that the Rh {Table S11, Figure S1(a)} and Pd catalysts (Table S10, Figure S1(b)} did not show a significant effect on the reaction was quite disappointing and will be explored further in future. A possible explanation for the lack of activity might lie in the lower concentrations used. It might also be due to the loss of nucleophilicity due to backbonding to the COD ligand.

[CO_2]-evaluation

The rate order of CO_2 was also evaluated by using different mole fractions of the gas with argon gas in the balloon setup (Fig. 11(d) and Fig. S16; Table S14). This was performed to determine if the CO_2 influenced the reaction rate or if it was zero-order.

The results (Table S15) illustrate that the conversion percentage and the k_{obs} are dependent on the amount of CO_2 present and increases linearly as the concentration of CO_2 was increased (Fig. 10). This indicates that the rate order of CO_2 is clearly first-order under the ideal reaction conditions.

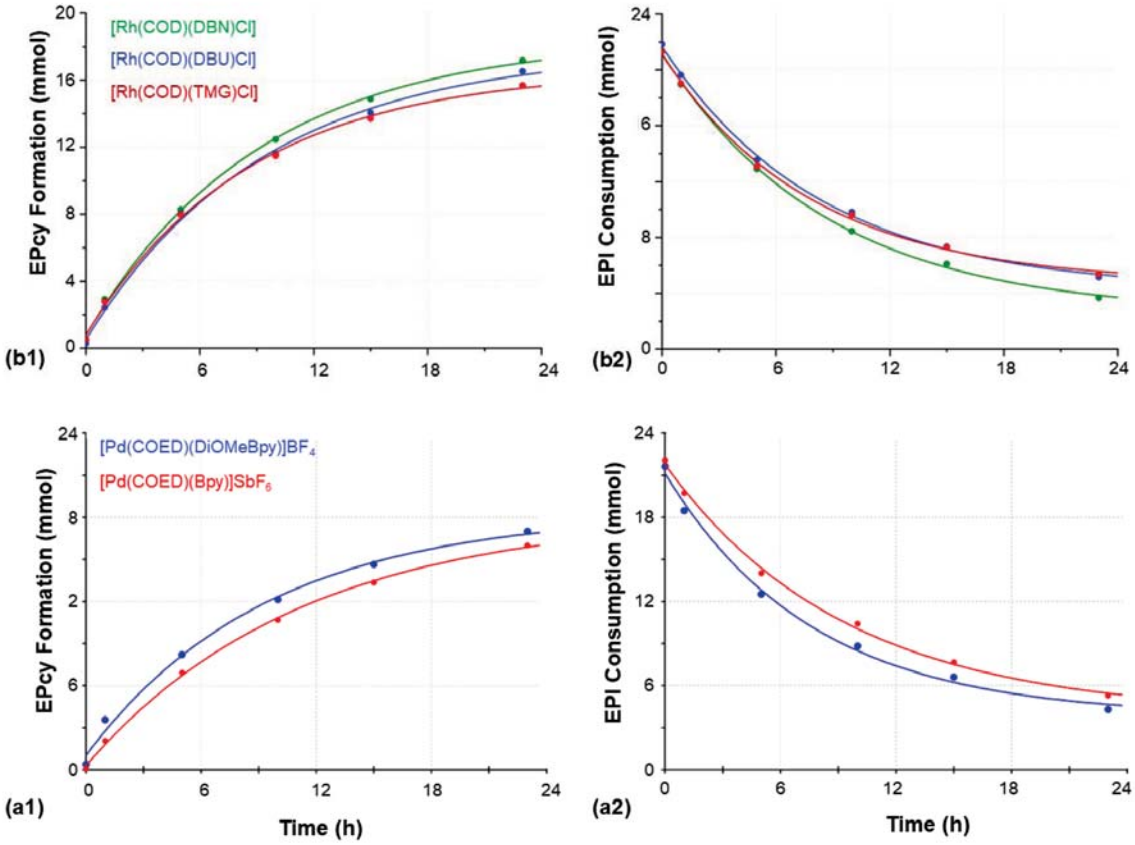

Figure 9: Illustration of the L.S. fits (Eq. 13) of EPcy formation and EPI consumption. Reactions are in the presence of different metals (a) ([Pd(COED)(DiOMeBpy)Me]BF_4 (**Pd-1**), [Pd(COED)(Bpy)]SbF_6 (**Pd-2**) Table S11, and (b) different metals [Rh(COD)(L)Cl] (**DBN**, **DBU** and **TMG**) Table S12. [EPI] = 22 mmol, [CO_2] = 1 atm (room temperature), [TBAI] = 2 mmol, [benzoic acid] =1 mmol, [Metal] = 0,025 mmol.

Proposed mechanism and rate law

Combination of all variables

The principal parameters influencing the rate of product formation as evaluated above are summarised in Figure 11. Individual rate and equilibrium data are given in Table 1 and 2.

The evaluation of the different parameters that influence the formation of a EPcy from the addition of CO_2 to an epoxide provided an array of insightful results. To aid the discussion of the results obtained, the summarised results (k_{obs}, conversion, TON and TOF) of the EPcy formation (Figs. 6-10) from EPI are provided in Tables 1 and 2, respectively.

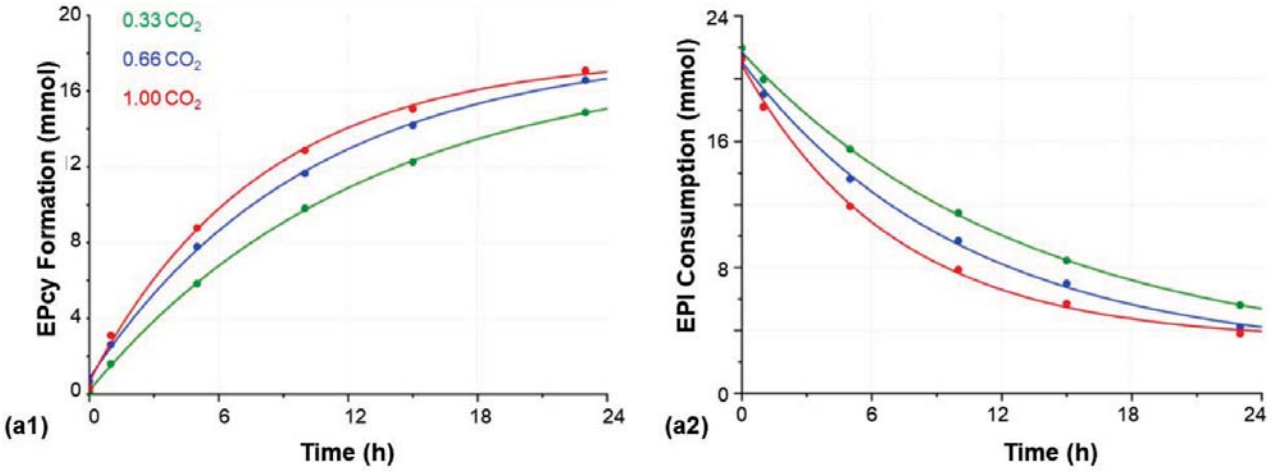

Figure 10: Illustration of the L.S. fits (Eq. 13) of (a) EPcy formation and (b) EPI consumption. Reactions are at different CO2 mole fractions at room temperature. [EPI] = 22 mmol, [TBAI] = 2 mmol, [benzoic acid] = 1 mmol, CO2 mole = 0,33 (138 mmol), 0,67 (285 mmol) and 1,00 (417 mmol). See Table S14 and Fig. 11(c).

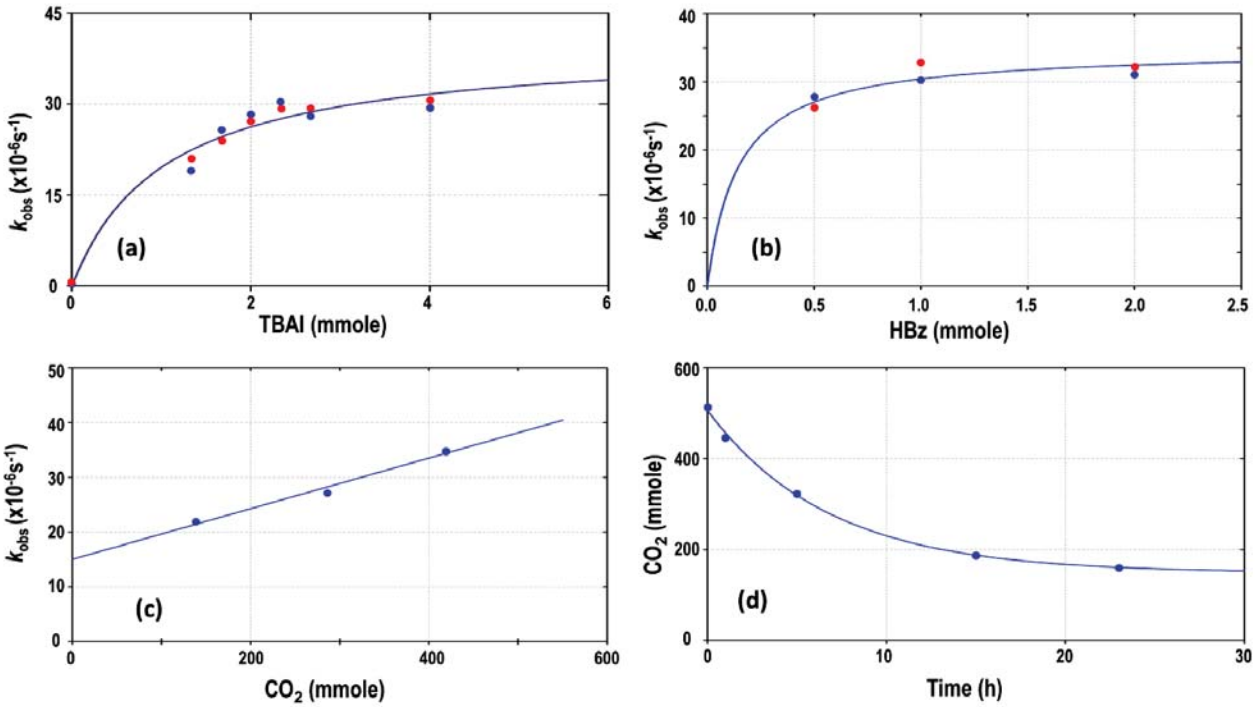

Figure 11: Graphical illustration of the principal parameters showing a direct influence on the observed rate constant (k_{obs}; from EPI reactant disappearance and EPcy product formation). Note that red indicates EPI disappearance while blue indicates cyclocarbonate (EPcy) formation. (a) Optimisation of the TBAI (L.S. fits to Eq. 9, as obtained from. Eqs. 1-7, and integration of Eq. 8, or more generally, [(EPcy), sien Tabel S5 and S7, asook Figuur 7(a)]. (b) Optimisation of benzoic acid (L.S. fits to Eq. 11, as obtained from from Eqs. 1-10) Table S9. (c) Illustration of L.S. fits (Eq. 15) of the observed rate constant (k_{obs}) *vs* the carbon dioxide (CO_2) concentration according to Eq. 15 and more generally Eq. 16. Reaction conditions: [EPI] = 22 mmol, [acid] = 1 mmol, [TBAI] = 2 mmol, CO_2 mole fractions = 0,33 (138 mmol), 0,67 (285 mmol) and 1,00 (417 mmol). See Table S14 and S15 and the resulting k_f (46 ± 8) $M^{-1}10^{-6}s^{-1}$ and k_r (15 ± 2) x $10^{-6}s^{-1}$, when fitted to Eq. 13, provided a K_{eq} value (Eq. 16) of (3,1 ± 0,7) M^{-1}. (d) Total CO_2 in the gas phase decrease during reaction. L.S. fit to Eq. 13 of the uptake/disappearance of CO_2 during the reaction of 25 mmol EPI, 2 mmol TBAI and 0,5 mmol ascorbic acid. The resulting observed rate constant (k_{obs}) was determined as (41 ± 5) x $10^{-6}s^{-1}$.

Table 1: Summary of k_{obs}, conversion, TON (conversion over 23h period) and TOF (conversion/h over 23h period) of the evaluated reaction conditions. Unless stated otherwise, the EPI concentration was 22 mmol, as illustrated in Figs. 6-11 and reported in Tables S2-S16.

Abbreviated Conditions	k_{wg} (x10^{-3}h^{-1})	k_{wg} (x10^{-6}s^{-1})	Conversion (%)	TON	TOF
1 TBAI 0,5 Control [a]	0 ± 10	0 ± 3	13,1	3	0,13
1 TBAI 0,5 Ascorbic [a]	35 ± 6	10 ± 2	38,5	8,4	0,36
1 TBAI 0,5 Benzoic [a]	37 ± 5	10 ± 1	31,5	7,1	0,31
1 TBAI 0,5 Succinic [b]	53 ± 2	15 ± 1	30,5	6,9	0,3
1 TBAI 0,5 Citric [b]	53 ± 2	15 ± 1	27,8	6,4	0,28
1 TBAI 0,5 Tarctaric [b]	29 ± 4	8 ± 1	26,3	6,1	0,27
1 TBAI 0,5 Metformin [b]	0 ± 5	0 ± 2	12,2	2,8	0,12
1 TBAI 0,5 Asc [c]	35 ± 6	10 ± 2	38,5	8,4	0,36
2 TBAI 0,5 Asc [c]	89 ± 4	25 ± 1	89,4	9,2	0,4
3 TBAI 0,5 Asc [c]	101 ± 5	28 ± 1	89,6	6,5	0,28
1 TBAI 0,5 Bz [d]	81 ± 5	19 ± 1	31,5	7,1	0,31
1,25 TBAI 0,5 Bz [d]	96 ± 14	27 ± 4	62,9	11	0,48
1,50 TBAI 0,5 Bz [d]	104 ± 15	29 ± 4	64,8	9,8	0,43
1,75 TBAI 0,5 Bz [d]	114 ± 14	32 ± 4	69,2	8,9	0,38
2 TBAI 0,5 Bz [d]	101 ± 10	28 ± 3	71,7	8	0,35
3 TBAI 0,5 Bz [d]	100 ± 8	28 ± 2	76,6	5,7	0,25
2 TBAI 1 Asc [e]	104 ± 6	29 ± 2	83,9	8,9	0,39
2 TBAI 2 Asc [e]	96 ± 15	27 ± 4	67,3	6,9	0,3
2 TBAI 1 Bz f, [h]	107 ± 14	30 ± 4	77,9	8,5	0,37
2 TBAI 2 Bz [f]	112 ± 11	31 ± 3	80,1	8,6	0,37
40 EPI 2 TBAI 1 Asc [g]	55 ± 8	15 ± 2	78,2	13,1	0,57
55 EPI 2 TBAI 1 Asc [g]	44 ± 3	12 ± 1	64,4	14,6	0,63
40 EPI 2 TBAI 1 Bz [h]	60 ± 10	17 ± 3	65,5	12,1	0,53
55 EPI 2 TBAI 1 Bz [h]	54 ± 10	15 ± 3	54,4	13,7	0,6
0.33 CO_2 2 TBAI 1 Bz [i]	78 ± 2	22 ± 1	67,4	7,4	0,32
0.67 CO_2 2 TBAI 1 Bz [i]	98 ± 5	27 ± 1	75	8,3	0,36
1,00 CO_2 2 TBAI 1 Bz [i]	126 ± 11	35 ± 3	79,2	8,5	0,37
1,00 CO_2 2 TBAI 1 Asc [j]	141 ± 11	41 ± 5	83,7	8,8	0,39

a) Fig. 6(b), Table S2; b) Fig. 6(a), Table S3; c) Fig. 7(b), Table S5; d) Fig. 7(a), Table S4; e) Fig. 8(a), Table S6; f) Fig. 8(b), Table S7; g) Fig. S17(a), Table S8; h) Fig. S17(b), Table S9; i) Fig. 11, Table S14; and j) Table S16.

Table 2: Summary of rate and equilibrium constants related to the Catalytic Scheme (Scheme 2) and Eqs. 1-4. The general reaction conditions were [EPI] = 22 mmol, [TBAI] = 2 mmol, [benzoic acid] = 1 mmol, [CO_2] = 1 atm (room temperature) – unless stated otherwise.

Constant/ Parameter	Experiment	Notes:
	TBAI plateau (Benzoic acid)	[TBAI] = 1-3 mmol
K_{eq}	(1150 ± 120) M^{-1}	Fig. 11(a)
k_1	(42 ± 5) x10^{-6}s^{-1}	Fig. 11(a)
	CO_2 rate constant determination	[CO_2] variation
K_{eq}	(3,1 ± 0.7) M^{-1}	Fig. 11(c)
k_f	(46 ± 8) M^{-1}10^{-6}s^{-1}	Fig. 11(c)
k_r	(15 ± 2) x10^{-6}s^{-1}	Fig. 11(c)
	Equilibrium constants	NB: Fig. 11
K_1	4x10^3 M^{-1}	Fig. 11(b)
K_2	1x10^3 M^{-1}	Fig. 11(a)
	Benzoic acid reaction influence	BenzH pK_a = 4,06
k_{wg} (TON, TOF) [a]	(28 ± 3) x 10^{-6}s^{-1} (8,0, 0,35)	2 mmol TBAI, 0,5 mmol acid
k_{wg} (TON, TOF) [a]	(30 ± 4) x 10^{-6}s^{-1} (8,5, 0,37)	2 mmol TBAI, 1 mmol acid
	Ascorbic acid reaction influence	AscH pK_a = 4,04
k_{wg} (TON, TOF) [a]	(25 ± 1) x 10^{-6}s^{-1} (9,2, 0,40)	2 mmol TBAI, 0,5 mmol acid
k_{wg} (TON, TOF) [a]	(29 ± 2) x 10^{-6}s^{-1} (8,9, 0,39)	2 mmol TBAI, 1 mmol acid

[a] "Turnover Number" and "Turnover Frequency"

Applicable reactions

The behaviour illustrated in Figure 11 can be translated into separate steps associated with the complete catalytic cycle and is highlighted below. Thus, based on the above variation of parameters the proposed reaction scheme of carbon dioxide capture by EPI with TBAI and benzoic acid allows the identification of four definite steps (see Eq. 1-4) and the corresponding catalytic cycle shown in Scheme 2. Note: as indicated in the text above, EPI=epichlorohydrin, while the iodide ion in Eq. 1-4 below is indicated as I.

$$\underset{A}{EpO} + H^+ \underset{k_{-1}}{\overset{K_1, k_1}{\rightleftharpoons}} \underset{B}{M/H^+Ep} \quad (fast) \qquad (1)$$

$$\underset{B}{M/H^+Ep} + I^- \underset{k_{-2}}{\overset{K_2, k_2}{\rightleftharpoons}} \underset{C}{M/HEpI} \quad (fast) \qquad (2)$$

$$\underset{C}{M/HEpI} + CO_2 \underset{k_{-3}}{\overset{K_3, k_3}{\rightleftharpoons}} \underset{D}{M/HEpICO_2} \quad (rds) \qquad (3)$$

$$\underset{D}{M/HEpICO_2} \underset{k_{-4}}{\overset{K_4, k_4}{\rightleftharpoons}} \underset{E}{CCarb} + M/H^+ + I^- \quad (fast) \qquad (4)$$

i. The first step (Eq. 1) defined by k_1 is considered to be the interaction/protonation of the epoxide by the acid
ii. Next, the iodide ion from the TBAI attacks the epoxide ring (k_2) to enable ring opening (Eq. 2).
iii. The carbon atom of the CO_2 is then attacked by the nucleophilic oxygen atom of the epoxide (k_3) and is followed by the ring closure (Eq. 3; rds = rate determining step).
iv. The final step (Eq. 4) is the regeneration of the acid and TBAI and formation of the EPcy (k_4).

Catalytic cycle

The catalytic cycle as described by the results above is shown in Scheme 2.

The data (see below) suggests an equilibrium present in intermediate steps, also inferred from the NMR spectra (Fig. S1 and 11(c)) which implies that there are intermediate species which are influenced by a change in TBAI and benzoic acid. All four the reactions (Eqs. 1-4), as identified in Scheme 2, are thus written as potential equilibria but are refined as discussed further below. The fact that all the reactions do not go to completion is a clear manifestation of the nett equilibrium present for the overall reaction sequence.

Based on (a) the parameters which displays observable effects on the rate constants (Fig. 11), (b) that which is known from literature (Guo et al., 2021), and (c) other general observations, the following is concluded for the catalytic cycle as illustrated in Scheme 2:

- In a series of consecutive reactions, the total reaction order of the process/combined reaction is determined by all reactions preceding the rate determining step. Clear influences on both the (i) Benzoic acid (Fig. 11(b)) and (ii) the TBAI (Fig. 11(a)) are observed, and since it is known that protonation/deprotonation (Eq. 1) as well as nucleophilic halide attack at the alpha carbon of an epoxide (Eq. 2) is usually very fast, (Guo et al., 2021) it is concluded that the subsequent attack by the ring-opened epoxide-O-atom on the C-atom at the carbon dioxide (Eq. 3) is most probably the rate-determining step (rds).
- Furthermore, since the subsequent *formation rate* of the (EPcy) product (E in Scheme 2), is the same (within the estimated standard deviations; see *e.g.* Figs. 6-10) as the disappearance of the reactant EPI, it may be concluded that the regeneration of the acid and the iodide ion, with the parallel and concurrent formation of the EPcy, is a fast process.

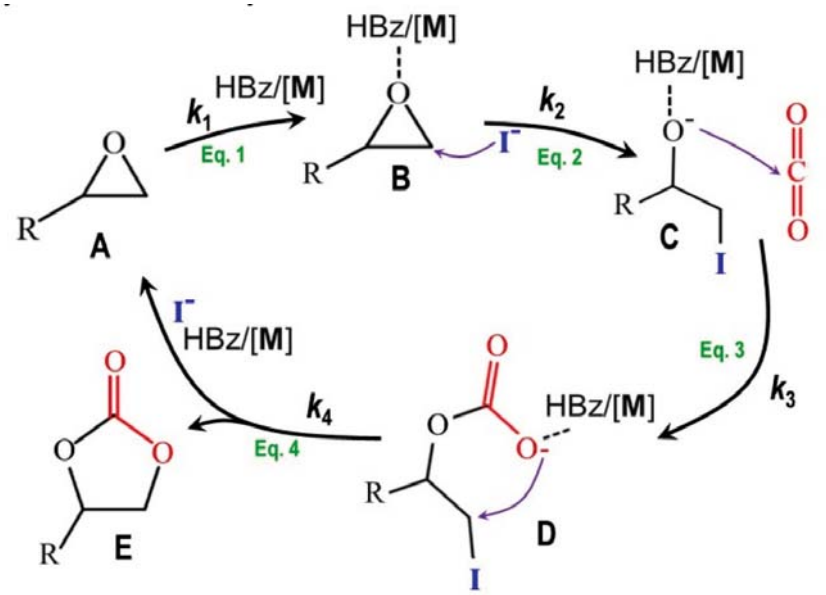

Scheme 2: Proposed catalytic cycle for the formation of EPcy (E) from EPI (A) in the presence of TBAI, benzoic acid and CO_2. Note that for simplicity only the forward steps are indicated in the cycle (see also Eqs. 1-4). Moreover, the benzoic acid is simply indicated as HBz ($[H^+]$ in Eqs. 1-4), and the TBAI as $[I^-]$, with the 'epoxide'-containing species as A, B, C and D, with the final cyclocarbonate product (EPcy) by E.

- The reaction profiles of -d[A]/dt / d[E]/dt *vs* [I^-] or [acid] both show limiting kinetics [formation of plateaus see Fig. 11(a) and (b); in agreement with Eqs. 8, 9 and 15], and indicate potential fast pre-equilibria associated with these steps (Eqs. 2 and 3). This is also inferred by the NMR data in Fig. S2. The equilibrium constants defined by Eqs. 2 and 3 are respectively $K_1 \approx 4x10^3$ M^{-1} and $K_2 \approx 1x10^3$ M^{-1}. Moreover, as indicated in above, the fact that none of the reactions go to completion is a clear manifestation of the equilibrium present for the overall reaction sequence.
- The observation above therefore justifies the assumption that under conditions as utilised in this study, the formation of the protonated species **B** is > 95% when [H^+] ≈ 0,7 mmol (Fig. 11(b)). However, the formation of species **C** wherein both the benzoic acid and the iodide are "secured", is only achieved at [I^-] ≈ 2 mmol, which is close to the saturation limit of the TBAI (Fig. 11(a)). Further experiments were therefore performed near this plateau, i.e., at approx. 1-2 mmol.
- Interesting to note from Fig. 11(c) is that upon variation of the carbon dioxide, both the -d[A]/dt and d[E]/dt *vs* [CO_2] display a *linear* relationship with a significant intercept. As indicated above, this step is assumed to be rate-determining. This intercept then suggests either (i) a parallel *concurrent* reaction or (ii) a *reversible* reaction associated with the intramolecular nucleophilic attack of the peroxide O-atom onto the carbon dioxide C-atom.
- As indicated above, there is clear evidence that the complete system is in *equilibrium*. If not, at lower [I^-], the conversion to the EPcy should have been close to quantitative. This is however clearly not the case, see Figs. 6-10. Assuming this, the overall equilibrium constant (K_{tot}) for the complete reaction is in the order of 5, implying that the overall reaction proceed only to a *ca*. 75% completion under the conditions studied.
- Finally, the small influence of the metal catalyst models of rhodium and palladium was disappointing, see Fig. 9. However, the concentrations were extremely low due to encountered solubility problems and will be explored further in the future. Hence, despite this negative comment, it may be noted that there is a tendency (although *small,* and not convincing at all; but still seemingly present) that (a) the Rh-complexes increase the rates, while (b) both the Pd- and Pt-complexes decreases the rate of the catalysis.

Derivation of the rate law

Next, taking all the above in account, an appropriate Rate Law may be derived, see Supplementary data. Only equations directly relevant to the discussion are included below.

The starting point is that since the uptake of the carbon dioxide (Eq. 3) is considered the rate-determining step, with the subsequent ring-closure and cyclocarbonate (EPcy) generation happening fast, one may write:

$$\frac{d[E]}{dt} = -\frac{d[A]}{dt}, \text{ and at time = t: } \frac{d[D]}{dt} = k_3[C]_t[CO_2] - k_{-3}[D]_t \quad (5)$$

The total concentration of epoxide (in different forms, A, B and C), just before Eq. 3 commences, is then given by:

$$[Ep]_{tot} = [C]_t + [B]_t + [A]_t \quad (6)$$

Since two equilibria for the reactions in Eq. 1 and 2 are assumed, upon inclusion in Eq. 6, it yields:

$$[C]_t = \frac{[Ep]_{tot}(K_1K_2[H^+][I^-])}{\{1+K_1[H^+]+K_1K_2[H^+][I^-]\}} \quad (7)$$

Substituting Eq.7 into Eq. 5 yields the following overarching rate law:

$$\frac{d[D]}{dt} = \frac{k_3[Ep]_{tot}[CO_2](K_1K_2[H^+][I^-])}{\{1+K_1[H^+]+K_1K_2[H^+][I^-]\}} - k_{-3}[\mathbf{D}]_t \quad (8)$$

Three general comments on the Rate Law and the individual dependences of reactants are therefore justified (noting that depending on which parameter is varied, the second order rate constants are indicated by k'_3, k''_3 and k'''_3, when varying [I^-], [H^+] and [CO_2], respectively):

- Considering the conditions selected in this study (from Fig. 11(b) it follows that $K_1[H^+]>>1$), and following integration, yields the observed rate constant k_{obs}, based on the disappearance of the EPI formation of the EPcy, assuming that $k'_3 = k_3K_2$:

$$k_{obs} = \frac{k'_3[CO_2][I^-]}{1+K_2[I^-]} + k_{-3} \quad (9)$$

Eq. 9 explains the observations made as indicated in Fig. 11(a), where [I^-] is varied while [H^+] and [CO_2] are kept constant. If the reverse reaction is negligible, or if it cannot be determined reliably, it could not be included in L.S. fits [Fig11(a) and b)].

- Moreover, by considering Eq. 8 under another set of conditions utilised in this study, i.e., at a *fixed* [TBAI]=2 mmol and *varying* the [Benzoic acid], the observed rate constant adheres to a system where a plateau is reached, yielding Eqs. 10 and 11, assuming K_2 being large [= (1150 ±120) M^{-1}; Fig. 11(b)]:

$$k_{obs} = \frac{k_3[CO_2][I^-]\,2K_1[H^+]}{1+K_2[I^-]+K_1[H^+]+2K_1[H^+]} + k_{-3} \quad (10)$$

Or:

$$k_{obs} = \frac{k''_3[CO_2][I^-]\,K_1[H^+]}{a+K_1[H^+]} + k_{-3} \quad (11)$$

It is clear that Eq. 11 also predicts the correct behaviour with respect to the addition of the acid as proton donor in the overarching process (see Fig. 11(c), with k_3" the rate constant associated with the complex rate law as derived, describing the important dependence on the carbon dioxide, catalyst (iodide anions), and acidity in total).

- Finally, by varying the [CO_2] while keeping the [I^-] and [H^+] at fixed values, but such that both $K_1[H^+]>>1$ and $K_2[I^-]>>1$, Eq. 12 is obtained, which describes the dependence of the observed rate constant on [CO_2] (see Fig. 11(c)).

$$k_{obs} = k'''_3[CO_2] + k_{-3} \quad (12)$$

Summarising comments

All relevant rate and equilibrium constants as obtained from the large number of experiments described above are summarised in Table 1 and 2.

The type of epoxide plays a critical role (Figure 1) and is illustrated by die significant rate constants difference observed between EPI and styrene oxide. It may point to the larger steric demand by the latter, which could inhibit the reaction.

One observation which is clear from Eq. 10 and the corresponding data presented in Fig. 11(c), with the slope given by k'''_3, is the unequivocal confirmation of an intercept, i.e., a *reverse step*, denoted by k_{-3}.

However, as alluded to above, the presence of an intercept could unfortunately neither be *convincingly* confirmed nor excluded by the data as presented when the (i) $[H^+]$ or (ii) $[I^-]$ was varied [see Fig. 11(a) and (b), respectively] due to factors such as the limited solubilities of different reactants, as well as the larger than normal observed estimated standard deviations of individual rate constants, brought about by limited NMR experiments required for each individual data point. This eliminated a large variation of the applicable parameters. Despite this seemingly negative comment, it is still concluded that the Rate Law (Eq. 8, with simplifications in Eqs. 9-11) as derived, based on the catalytic cycle (Scheme 2) as proposed, is a *good representation* of the behaviour of the complex system based on the extensive kinetic runs reported in this study. All tendencies as observed in the extensive experiments are explained by the rate law.

The varying k_{obs} values and conversion rates observed for the different acids shown in Fig. 6 indicate that the pK_a value is not the only parameter that influences the reaction but also the Brønsted acidity and number of acidic protons. This is in agreement with literature (Watt et al., 2021) (Arayachukiat et al., 2017) where TBAI with ascorbic acid (4 acidic protons, pK_a = 4,04 – relative to the most acidic proton) and an ascorbic acid derivative with 2 acidic protons (pK_a = 4,06) resulted in an EPI conversion of 70% and 58%, respectively. However, two additional ascorbic acid derivatives with 1 and 2 acidic protons, respectively, resulted in an EPI conversion of 74% and 80% (both p$K_a \approx$ 11,3 – estimation based on ascorbic acid), which illustrates that the pK_a potentially plays a larger role than the number of acidic protons (Watt et al., 2021) (Arayachukiat et al., 2017). This is further corroborated, in the same article, where phenol (pK_a = 9,90) yielded a conversion of 87%. This may account for the lower conversions (Table S3; Figure 6) for succinic, tartaric and citric acid which have acidic protons with pK_a values lower than ascorbic and benzoic acid.

The relationship between ascorbic and benzoic acid (0,5 mmol acid) with various TBAI concentrations (Table S4, S5; Fig. 7), namely 1, 2 and 3 mmol, showed that the conversion plateaued for ascorbic acid from 2 mmol TBAI (89,4% and 89,6%, respectively), while the conversion with benzoic acid still increased somewhat beyond 2 mmol (71,7% and 76,6%, respectively) (Fig. 11). The inverse occurred for the k_{obs}, where it increased beyond 2 mmol for ascorbic acid ($(25 \pm 1) \times 10^{-6} s^{-1}$ and $(28 \pm 1) \times 10^{-6} s^{-1}$, respectively) and plateaued with benzoic acid ($(28 \pm 3) \times 10^{-6} s^{-1}$ and $(28 \pm 2) \times 10^{-6} s^{-1}$, respectively). Interestingly, benzoic acid ($(28 \pm 3) \times 10^{-6} s^{-1}$) had a larger k_{obs} than ascorbic acid ($(25 \pm 1) \times 10^{-6} s^{-1}$) but a smaller conversion (71,7% and 89,4%, respectively). The best comparable TON for ascorbic and benzoic acid (0,5 mmol acid) was with 2 mmol TBAI (9,2 and 8,0, respectively).

The results from increasing the acid concentration (0,5, 1 and 2 mmol) relative to 2 mmol TBAI (Table S4, S5) saw an increase in the conversion (71,7%, 77,9% and 80,1%, respectively) and k_{obs} ($(28 \pm 3) \times 10^{-6} s^{-1}$, $(30 \pm 4) \times 10^{-6} s^{-1}$ and $(31 \pm 3) \times 10^{-6} s^{-1}$, respectively) for benzoic acid, while ascorbic acid saw a decrease in conversion (89,4%, 83,9% and 67,3%, respectively). The ascorbic acid k_{obs} behaved differently by increasing from $(25 \pm 1) \times 10^{-6} s^{-1}$ to $(29 \pm 2) \times 10^{-6} s^{-1}$, then decreasing to $(27 \pm 4) \times 10^{-6} s^{-1}$. The conversion might suggest that at an ascorbic acid concentration of 0,5 mmol and 2 mmol TBAI there is an equivalent number of acidic protons (four per ascorbic acid) to the TBAI. When the acid concentration is increased there is a "surplus" of protons that then might inhibit the reaction. While literature suggests that the number of acidic protons plays a role in the reaction, no evaluation of a single acid with multiply acidic protons and at different concentrations relative to a specific TBAI concentration has been performed (Hill & Roodt, 2018) (Redgard, 2021) (Roodt et al., 2022).

When the reactions for both acids (0,5 mmol) were performed with 2 mmol TBAI in different EPI concentrations of approximately 22 mmol, 35 mmol and 50 mmol (Fig. S17, Table 1), the normalised values *relative to 25 mmol* gave virtually identical k_{obs} values for ascorbic acid ($(24 \pm 2) \times 10^{-6} s^{-1}$, $(20 \pm 3) \times 10^{-6} s^{-1}$ and $(22 \pm 2) \times 10^{-6} s^{-1}$) and similarly for benzoic acid ($(26 \pm 4) \times 10^{-6} s^{-1}$, $(24 \pm 4) \times 10^{-6} s^{-1}$ and $(30 \pm 6) \times 10^{-6} s^{-1}$), in increasing order of their EPI concentrations, respectively. This confirmed that the rate constants were all equal within estimated standard deviations, and illustrated the first-order dependence of the rate constants on [EPI] as reactant.

The rate order of CO_2 was also determined to be first order (Fig. 10 and 11(c), Table 1) as shown by the mole fractions of 0,33 (138 mmol), 0,67 (285 mmol) and 1,00 (417 mmol) that gave k_{obs} values of $(22 \pm 1) \times 10^{-6} s^{-1}$, $(27 \pm 1) \times 10^{-6} s^{-1}$ and $(35 \pm 3) \times 10^{-6} s^{-1}$, respectively.

Of the metal catalysts evaluated the rhodium complexes faired the best, followed by the palladium. Evidence has shown that **DBN**, **DBU** and **TMG** are excellent CO_2-trapping agents, and this may be the reason for the improved k_{obs} values noted (Redgard, 2019) (Yoshida et al., 2018). The use of DBU as a nucleophile in similar epoxide reactions with TBAI and no acid showed activity (Guo et al., 2021). However, the reduced conversion rates could be because of the strong basicity of these ligands deprotonating the acids. The palladium complexes performed the worst and may be due to either the addition of iodide to the complexes or protonation of the η^3-allyl bond.

While a reaction scheme has previously been proposed in literature, a thorough investigation to develop the *rate law* of the reaction has not been noted previously (Watt et al., 2021) (Dolai et al., 2020) (Guo et al., 2021). Given that the reaction was performed with ambient CO_2 pressure, it is easily understood why it is the rate-determining step in the reaction and literature has shown improved results at higher pressures, as well as temperatures.

In reality, when (i) the activation energy of simple substitution processes are considered, as well as (ii) the increased pressure and higher temperatures employed in literature (Pescarmona, 2021) the values for the CO_2 captured as reported here are identical. It was however clearly illustrated by this study, when carefully and systematically taking all relevant parameters into consideration, a more complete experimental approach is possible, and may yield more informative, and most likely *more reliable* results than pure product analysis.

Conclusions

The homogeneously catalysed CO_2 capture via cycloaddition to epichlorohydrin (EPI) as epoxide allowed accurate and detailed *kinetic-mechanistic* analysis via time-resolved ^{1}H NMR, displaying simple first-order kinetics with respect to [EPI]. It provided significant insight into the reaction mechanism which has not been previously performed in such depth.

Several parameters were carefully evaluated, including a range of acids based on literature (Yingcharoen et al., 2019), with ascorbic acid and benzoic acid identified as target performers. Next, the TBAI (tetrabutylammonium iodide) and [EPI] were systematically optimised, while the CO_2 concentration changes, under atmospheric pressure, were investigated.

The PGM complexes [Rh(COD)(L)Cl] (L = DBN, DBU, TMG), [Pd(COED)(N,N')]X and [Pt(COD)(N,N')Me]X disappointingly indicated only slight activity (Rh), or slight deactivation (Pd), contrary to initial expectations, and identified the iodide ion as the principal catalyst.

The results from the investigation led to the successful development of a proposed reaction scheme (both stoichiometric and catalytic) and rate law with four definite steps identified. It suggests that the ring-opening of the epoxide is most probably the rate-determining step, yielding the expression (k_{obs}) for the disappearance of the epoxide, associated with an overall order of 4.

While this study provided significant insight into the parameters that influence the formation of cyclocarbonates from the CO_2 capture by an epoxide and, there is more that needs to be assessed to fully understand the system. An important point would be the relationship between the acid and TBAI. Moreover, the effects of metal centres need to be broadened significantly. It is also important that a comprehensive theoretical study is conducted to obtain further information with regard to the range of parameters evaluated in this study. A start with a preliminary study has already been made.

Additional evaluation of this system with other epoxide substrates will also probably yield additional clarity on the requirements to produce value-added products with CO_2.

Although some limitations on the experiments were encountered, this study still concluded that the Rate Law as derived, based on the catalytic cycle (Scheme 2) as proposed, is an excellent representation of the behaviour of the complex system as studied. It also confirmed the significant dependence of the reaction on acid, epoxide and TBAI, as well as the CO_2 and pressure. Moreover, it concluded this via a detailed kinetic-mechanistic investigation and quantitively explained why the rate law is a fourth-order process.

Experimental section

Ligands for metal complexes

The rhodium complexes synthesised were used to evaluate the (added) catalytic performance with epoxides and CO_2 (Redgard, 2019). The basis of the complexes was to evaluate the influence that various N,N' ligands, specifically 2,2'-bipyridine analogues (Fig. 12), have on the structure and their use as catalysts.

Chemicals and Instrumentation

All reagents and solvents used for the synthesis and preparation of the complexes were of analytical grade, purchased from Sigma-Aldrich, South-Africa and were used without further purification, unless stated otherwise. When anhydrous conditions were required, solvents were purified and dried according to literature procedures (Armarego, 2017). Selected complexes that were synthesised were characterised by elemental analyses from Atlantic Microlab, Inc., Norcross,

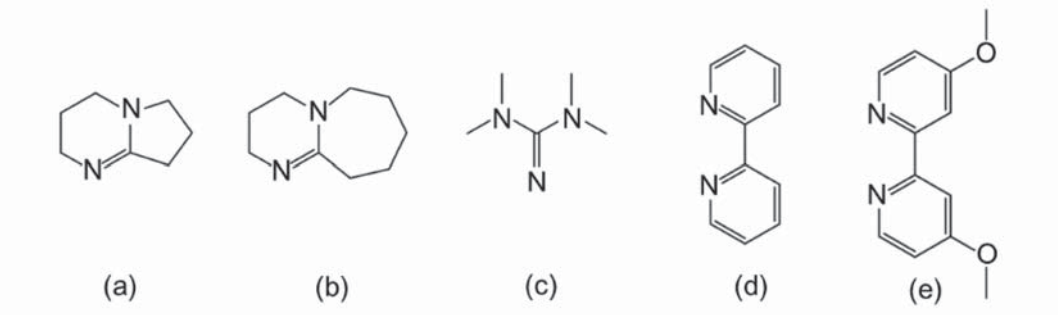

Figure 12: Structures of the ligands used for the Rhodium and Palladium complexes: (a) 1,5-diazabicyclo[4.3.0] non-5-ene (DBN), (b) 1,8-diazabicyclo[5.4.0]undec-7-ene (DBU) and (c) 1,1,3,3-tetramethylguanidine (TMG). (d) 2,2'-bipyridine (Bpy), (e) 4,4'-dimethoxy-2,2'-bipyridine (DiOMeBpy).

Georgia, USA. The infrared spectra of the complexes were analysed using the ATR sampling technique on a Thermo Scientific Nicolet iS10 FT–IR spectrophotometer with a laser range of 4000–400 cm^{-1} and are reported in cm^{-1}. The ^1H and ^{13}C NMR spectra were collected on a 600 MHz Bruker Avance II 600 (^1H: 600 MHz, ^{13}C: 151 MHz) spectrometer and the chemical shifts (δ), reported in ppm, were relative to tetramethylsilane (TMS). The ^1H and ^{13}C spectra were referenced internally with respect to the residual peaks of the corresponding deuterated solvent (C_6D_6: 7,14 ppm, 127,7 ppm; $(CD_3)_2CO$: 2,06 ppm, 29,00 ppm and $CDCl_3$: 7,28 ppm, 77,0 ppm, respectively).

The epoxides were purchased Sigma-Aldrich, South-Africa and used as received. Typical details of ^1H data is as follows (see Fig. 1 for numbering of protons):

Epichlorohydrin (EPI). ^1H NMR ($CDCl_3$, 600 MHz): δ 3,56-3,51 (m, 1H), 3,40-3,35 (m, 1H), 3,12-3,07 (m, 1H), 2,77-2,73 (m, 1H), 2,58-2,53 (m, 1H)

Cyclocarbonate (EPcy). ^1H NMR ($CDCl_3$, 600 MHz): δ 5,05-5,00 (m, 1H), 4,6-4,53 (m, 1H) 4,36-4,31 (m, 1H), 3,82-3,77 (m, 1H), 3,74-3,69 (m, 1H)

Synthetic procedures

The synthesis procedures that are discussed below address the formation of the precursor complexes that were required for the reaction to form the desired Pd-complexes. This was followed by the synthesis of the rhodium and palladium complexes, respectively. Note that the structures of the five complexes [Rh(COD)(DBN)Cl] (**DBN**), [Rh(COD)(TMG)Cl] (**TMG**) [Rh(COD)(DBU)Cl] (**DBU**), [Pd(COED)(DiOMeBpy)]BF_4 (**Pd-1**), and [Pd(COED)-(Bpy)]SbF_6 (**Pd-2**) have been previously reported and have been appropriately characterised (Redgard, 2021) (Roodt, Venter, & Redgard, 2022).

Precursor Pd(COD) complexes.

The formation of the precursor complexes {[M(COD)Cl_2] (Enders, et al., 2014) (Štěpnička & Císařová, 1996) and [M(COD)(Me)Cl] (Dekker, et al., 1992) (M = Pd)} were based on literature procedures. Characterisation by ^1H and ^{13}C NMR agreed with literature and thus sufficed to ensure correct and pure compounds were obtained.

[Pd(COD)Cl_2]. [$PdCl_2$] (2 g, 11,28 mmol) was dissolved in hot concentrated HCl (6 ml, 10 M) and stirred for 15 minutes. The solution was then left to cool to room temperature, diluted with ethanol (150 ml) and filtered. An excess of 1,5-cyclooctadiene (COD) (2,8 ml, 23 mmol) was added to the filtrate and stirred rapidly for 15 minutes. The solution was then filtered, and the precipitate was washed with diethyl ether (100 ml). The product was a yellow powder (2,97 g, 92%), ^1H NMR ($CDCl_3$, 600 MHz): δ 6,38-6,29 (m, 4H), 3,00-2,88 (m, 4H), 2,65-2,52 (m, 4H), ^{13}C NMR ($CDCl_3$, 151 MHz): δ 116,7, 31,0.

[Pd(COD)(Me)Cl]. [Pd(COD)Cl_2] (280 mg, 1 mmol) was added to a mixture of DCM/Methanol (1:1, 20 ml), followed by 1,2 eq. of tetramethyltin (170 µl, 1,2 mmol). The reaction mixture was left to stir at room temperature for 24 hours. The solution was then dried and washed with diethyl ether (50 ml). The product was a grey-white powder (230 mg, 88%). Recrystallisation attempts were not successful. *Anal.* Calculated for $PdC_{11}H_{21}Cl$ (%): C, 44,76; H, 7,17, Found: C, 38,73; H, 5,66, ^1H NMR (Acetone-d^6, 600 MHz): δ 5,83-5,75 (m, 2H), 5,26-5,18 (m, 2H), 2,73-2,62 (m, 4H), 2,58-2,43 (m, 4H), 1,01 (s, 3H), ^{13}C NMR (Acetone-d^6, 151 MHz): δ 123,8, 101,6, 30,8, 27,3, 9,41.

Synthesis of the [Rh(COD)(L)Cl] complexes.

The synthesis procedure (Scheme 3) of the rhodium(I) complexes was all identical for the coordination of DBN, DBU and TMG, respectively (see Fig. 12 for structures and names) (Flörke et al., 1992). [Rh(COD)$_2$$Cl_2$] (0,20 mmol) was dissolved in dioxane (15 ml), followed by the appropriate base (2 eq.), stirred at room temperature for 18 hours and dried to yield a powder.

[Rh(COD)(DBN)Cl] (DBN). 1,5-diazabicyclo[4.3.0]non-5-ene, DBN, (50 µl, 0,40 mmol) was added to a dioxane solution containing [Rh(COD)$_2$$Cl_2$] (100 mg, 0,20 mmol) to yield the [Rh(COD)(DBN)Cl] complex (110 mg, 77%). IR (cm^{-1}): $\nu_{(C=N)}$ = 1650. ^1H NMR (C_6D_6, 600 MHz): δ 4,95 (s, 2H), 3,54 (s, 2H), 3,24-3,14 (br, 2H), 3,04-2,88 (br, 2H), 2,37 (t, 2H), 2,36-2,28 (br, 4H), 2,23 (t, 2H), 1,64 (d, 4H), 1,27-1,21 (m, 2H), 1,21-1,16 (m, 2H), ^{13}C NMR (C_6D_6, 151 MHz): δ 162,3, 82,7 (d), 72,8 (d), 51,4, 45,7, 41,8, 33,2, 31,7, 30,5, 20,6, 18,9.

[Rh(COD)(TMG)Cl] (TMG). 1,1,3,3-tetramethylguanidine, TMG, (50 µl, 0,40 mmol) was added to a dioxane solution containing [Rh(COD)$_2$$Cl_2$] (100 mg, 0,20 mmol) to yield the [Rh(COD)(TMG)Cl] complex (130 mg, 86%).

IR (cm^{-1}): $\nu_{(C=N)}$ = 1567, 1527. ^1H NMR (C_6D_6, 600 MHz): δ 4,87 (s, 2H), 3,60 (s, 2H), 3,14 – 2,66 (br, 6H), 2,38 – 2,29 (br, 4H), 2,25 – 1,80 (br, 6H), 1,63 (d, 4H), ^{13}C NMR (C_6D_6, 151 MHz): δ 170,6, 80,8 (d), 73,4 (d), 40,8 – 39,3, 38,5 – 37,3, 31,5, 30,7.

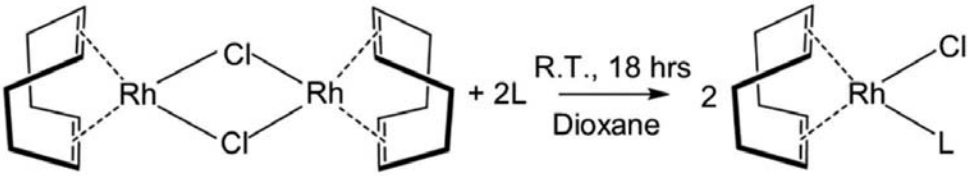

Scheme 3: The general reaction scheme for the synthesis of different [Rh(COD)(L)Cl] complexes (L = DBN, DBU and TMG). See Fig. 15 for structures and names of L.

[Rh(COD)(DBU)Cl] (DBU). 1,8-diazabicyclo[5.4.0]undec-7-ene, DBU, (60 µl, 0,40 mmol) was added to a dioxane solution containing $[Rh(COD)_2Cl_2]$ (100 mg, 0,20 mmol) to yield the [Rh(COD)(DBU)Cl] complex (150 mg, 90%). IR (cm^{-1}): $\nu_{(C=N)}$ = 1606. ^1H NMR (C_6D_6, 600 MHz): δ 4,98 (s, 1H), 4,89 (s, 1H), 3,64 (s, 1H), 3,57 (s, 1H), 3,51 (s, 1H), 3,43 (s, 1H), 3,11 (s, 1H), 2,96 (s, 1H), 2,48 – 2,22 (m, 8H), 1,94 (s, 1H), 1,67 (s, 2H), 1,59 (s, 2H), 1,53 (s, 1H), 1,46 (s, 1H), 1,27 (s, 1H), 1,27 (s, 1H), 1,15 (s, 2H), 0,95 (s, 1H), 0,92 (s, 1H), ^{13}C NMR (C_6D_6, 151 MHz): δ 163,0, 82,6 (d), 81,6 (d), 73,1 (d), 72,9 (d), 52,5, 46,9, 46,8, 39,0, 31,9, 31,3, 30,7, 30,4, 29,0, 27,3, 25,0, 22,0.

Synthesis of [Pd(COED)(N,N')]X complexes

The synthesis procedure (Scheme 4) of the palladium(II) complexes were identical for the coordination of Bpy, and DiOMeBpy (see Fig. 12 for structures and names) with the respective counterions. (Bianca et al., 2002) (Armarego, 2017).

[Pd(COD)(Me)Cl] (0,377 mmol) was dissolved in 20 ml dry THF, followed by $Ag[SbF_6]$ (0,377 mmol), and left to stir for 30 minutes. The solution was filtered and 1 eq. of the corresponding N,N' ligand (Bpy, DiOMeBpy and DitBuBpy) was added to the filtrate and stirred at room temperature for 28 hours. The solution was dried, dissolved in DCM and filtered and left to recrystalise. For the reaction with $Ag[BF_4]$ the solvent was acetone.

[Pd(COED)(DiOMeBpy)]BF_4 (Pd-1). 4,4'-dimethoxy-2,2'-bipyridine, DiOMeBpy, (80 mg, 0,38 mmol) was added to the filtrate of [Pd(COD)(Me)Cl] (100 mg, 0,38 mmol) and $Ag[BF_4]$ (70 mg, 0,38 mmol) dissolved in dry THF to yield [Pd(COED)(DiOMeBpy)]BF_4 (170 mg, 84%). Crystals suitable for SC-XRD analysis were formed. IR (cm^{-1}): $\nu_{(C=N)}$ = 1613. ^1H NMR (Acetone-d^6, 600 MHz): δ 8,96 (d, 2H, *J* = 6,3 Hz), 8,21 (d, 2H, *J* = 2,6 Hz), 7,36 (dd, 2H, *J* = 6,3, 2,6 Hz), 5,91 (t, 1H, *J* = 8,1 Hz), 5,08 (q, 2H), 4,16 (s, 6H), 2,63-2,56 (m, 2H), 2,34-2,25 (m, 2H), 1,71-1,64 (m, 2H), 1,31-1,25 (m, 3H), 0,91 (d, 3H, *J* = 6,7 Hz). ^{13}C NMR (Acetone-d^6, 151 MHz): δ 168,7, 155,4, 154,4, 113,1, 111,4 110,0, 76,5, 56,5, 33,9, 29,6, 27,8, 21,4.

[Pd(COED)(Bpy)]SbF_6 (Pd-2). 2,2'-bipyridine, Bpy, (60 mg, 0,38 mmol) was added to the filtrate of [Pd(COD)(Me)Cl] (100 mg, 0,38 mmol) and $Ag[SbF_6]$ (130 mg, 0,38 mmol) dissolved in dry THF to yield [Pd(COED)(Bpy)]SbF_6 (150 mg, 65%). Crystals suitable for SC-XRD analysis were formed. *Anal.* Calculated for $PdC_{21}H_{29}N_2F_6Sb$ (%): C, 38,71; H, 4,49; N, 4,30. Found: C, 39,17; H, 4,34; N, 4,39. IR (cm^{-1}):$\nu_{(C=N)}$ = 1599. ^1H NMR (Acetone-d^6, 600 MHz): δ 9,21-9,17 (m, 2H), 8,70 (d, 2H, *J* = 8,1 Hz), 8,40 (td, 2H, *J* = 7,9, 1,7 Hz), 7,88-7,84 (m, 2H), 5,99 (t, 1H, *J* = 8,2 Hz), 5,18 (q, 2H), 2,67-2,60 (m, 2H), 2,38-2,28 (m, 2H), 1,72-1,64 (m, 2H), 1,33-1,24 (m, 3H), 0,91 (d, 3H, *J* = 8,1 Hz). ^{13}C NMR (Acetone-d^6, 151 MHz): δ 154,7, 154,3, 140,9, 128,0, 123,5, 112,3, 77,5, 33,8, 29,6, 27,8, 21,3.

Carbon dioxide capturing experiments

All the reagents were purchased from Sigma-Aldrich, of analytical grade and used without further purification. The ^1H NMR kinetics was performed on a Bruker Avance II 600 (600MHz) spectrometer and the chemical shifts (d) were recorded relative to tetramethylsilane (TMS) and reported in ppm. All the ^1H NMR spectra were performed at room temperature, in deuterated chloroform and internally referenced using the residual protons of the deuterated solvent ($CDCl_3$: 7,29 ppm). The integrations and illustrations of the ^1H NMR kinetics spectra were done using Bruker TopSpin (Bruker, 2021) and OriginPro (OriginLab, 2021) was used for data-fitting and illustrations.

The synthesis procedure for the formation of the EPcy from EPI and CO_2 was performed at room temperature for 23 hours with a balloon setup and solvent-free. The reaction conditions were evaluated and optimised as reported above based on the procedure from literature (Dolai et al., 2020) and determined to be: [EPI] = 22 mmol, [TBAI] = 2 mmol, [Benzoic acid] = 1 mmol, [CO_2] = 1 atm (TBAI = tetrabutylammonium iodide). The yield was determined from ^1H NMR spectroscopy by calibration using the methyl protons of TBAI and found to be 17,1 mmol (77,9%, TON = 8,5, TOF = 0,37 h^{-1}). The experimental procedure and the protocol to collect the ^1H NMR spectra were consistent throughout the data reported in this manuscript.

The kinetic experimental conditions used in this work was to extract an aliquot (100 µl) of the reaction mixture and dissolve it in deuterated chloroform (500 µl). Four reactions were performed in duplicate and in unison and ^1H NMR characterisation was taken at 0, 1, 5, 10, 15 and 23 hours. The proton peaks of the reactant and product were calibrated with respect to the methyl protons of TBAI. This is illustrated in the ^1H NMR spectra (Figs. 2-3) where the molar ratio between the TBAI and the epoxide was 2:20, and the peaks indicated by the red arrow were used to assess the formation, consumption, and calibration respectively.

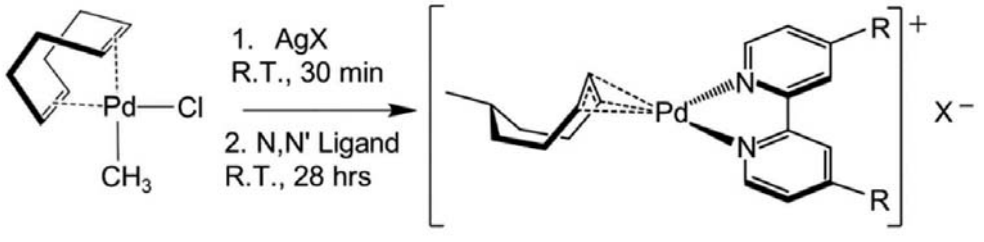

Scheme 4: The general reaction scheme for the synthesis of different [Pd(COED)(N,N')]X complexes (X = SbF_6^-/BF_4^-). COED = η^3-6-methylcyclooct-2-en-1-id.

Given that TBAI has 12 methyl protons and that both the product and reactant have discernible proton peaks that each integrate for one, then calibrating the spectra to 24 will indicate the amount (mmol) of the product and reactant that is present. The peaks used to measure the reaction were selected due to them being the most isolated peaks. In addition, the spectra in Fig. 2-3 represent the reactant and cleaned product ^{1}H-NMR spectra which were used to study the kinetics and confirm the product formation. Fig. 2(d) shows the presence of TBAI and the product, which agrees with the cleaned product (Fig. 2(b)).

The balloon setup (ensuring ambient pressure, *i.e.*, 1 atm; see also Figure S16) of the reaction using polyethylene balloons rather than latex balloons [loss of CO_2 from Latex was ca. 10x faster than from the polyethylene ones. To illustrate: latex balloons being completely deflated after 5 hours, whereas the polyethylene balloons still retained significant amounts of CO_2 after 1 day. The deflation of the CO_2-filled balloons over the reaction period is illustrated Table S16 and Fig. 2(d) with two reaction setups. To determine the amount (mmol) of CO_2 present in the balloons, the circumference was measured, and the volume determined S16). The loss of CO_2 over the reaction time (Fig. 11(d)) shows that there is still a significant amount of CO_2 escaping the system even though measures were taken to seal the balloon with tape and parafilm, with an observed rate constant (k_{obs}) of (41 ± 5) x10^{-6}s^{-1}. Nevertheless, the constant pressure during the use of ambient CO_2 pressures allows for simplified reaction conditions and highlights the efficacy of the reactions without the needs of energy/cost-intensive equipment – which is a barrier in industrial application.

Treatmeny of kinetic data

A modified Beer-Lambert law was used in the exponential form for the pseudo first-order rate constant (k_{obs}), in term of time-resolved NMR data as obtained from the signal integrals, (Eq. 13) (Purcell et al., 1989) (Leipoldt et al., 1983) (Smit et al, 1993) (Van der Westhuizen et al., 2010). This involved the least-squares fitting of the subsequent data to yield k_{obs}. The reaction progress described in in this study was evaluated by measuring the reactant disapprearance/ product formation (in mmol) *via* time-resolved ^{1}H-NMR spectroscopy and fitting/ reporting both of these processes.

$$B_t = B_\infty - (B_\infty - B_0)e^{-k_{obs}t} \quad (13)$$

Here B_t and B_∞ represent the NMR signal integrals, directly proportional to the concentrations of the reactants and product entities (e.g., mmol) after time *t* (hours/minutes/seconds) and infinite time, respectively, with B_∞ reached at the time which the reaction is, for practical purposes, complete.

Obviously, when subjecting the measurable entity (Absorbance, NMR peak height, IR peak intensity, etc.) which defines the reaction progress, to Eq. 13 via a least-squares fit, it can be easily ascertained whether the process is first order, by comparing the calculated values with the observed ones.

However, when not many data points of the process are available, it is sometimes also beneficial to rather use the natural logarithmic form of Eq. 13, as shown in Eq. 14. Obtaining a straight line (see Fig. 5(a)) is thus considered additional good evidence of the first order behaviour associated with such a process, where the slope of the line then yields the pseudo first-order rate constant, k_{obs}.

$$ln[B]_t = -k_{obs}t + ln[B]_0 \quad (14)$$

In Eq. 14, [*B*] represents the concentration equivalent (or measurable entity of reactant *R*, directly proportional to the concentration thereof) at time *t* and time zero, respectively.

Furthermore, the pseudo first-order rate constant (k_{obs}) under equilibrium conditions can then, for example, be expressed with respect to different contributing reactant concentrations (R_1, R_2), and when $[R_1]>>[R_2]$, often yields the relationship as shown in Eq. 15.

$$k_{obs} = k_f[R_1] + k_r \quad (15)$$

The slope (k_f) and the y-intercept (k_r) of the resulting graph using Eq. 15 typically reveal the forward (second order) and reverse (first order) rate constants, respectively, from which the 'kinetic' equilibrium constant can then also be obtained (Eq. 16).

$$K_{eq} = \frac{k_f}{k_r} \quad (16)$$

The equilibrium constant K_{eq} may also be obtained under favourable conditions, such as when a fast equilibrium precedes a rate determining step (k_1), from a least-squares fit of the first-order rate constant (k_{obs}) *vs* reactant (R) concentrations as given in Eq. 17.

$$k_{obs} = \frac{k_1 K_{eq}[R]}{1+K_{eq}[R]} \quad (17)$$

Supporting information

Supporting information is available from the authors. For appropriate literature therein see Table S1 and Figure S15 (Guil-López et al., 2019) (Büttner et al., 2017) (Lamb, 2019) (Dolai et al, 2020) (Guo et al., 2021) (Martin et al., 2015) (Pescarmona & Tahermehr, 2021).

Acknowledgements

Financial assistance from the University of Zürich and the University of the Free State is gratefully acknowledged. We thank the Swiss National Science Foundation (SNF Project IZLSZ2_149029/1) and the South African National Research Foundation (SANRF) (AR: UID: 107802), the Competitive Program for Rated Researchers of the SANRF (AR: UID 111698), as well as from the Competitive Program for Unrated Researchers of the SA NRF (J.A.V.: 116302) for financial support. Gratitude is also expressed to the Suid-Afrikaanse Akademie vir Wetenskap and Kuns for awarding the M.T. Steyn Prize to A.R., which enabled him to complete this project (SA-Akademie-vir-Wetenskap-en-Kuns, 2023). SASOL, Dr Gerdus Kemp and Klydon Pharmaceuticals (Grant no: WD 99139) are also thanked for financial support. Opinions, findings, conclusions or recommendations expressed in this material are those of the authors and do not necessarily reflect the views of the SANRF.

Author declaration

Conceptualisation, A.R.; methodology, A.R. and J.A.V.; software, A.R.; validation, S.R, A.R., J.A.V.; formal experiments, S.R; investigation, S.R; resources, A.R. and J.A.V.; data curation, S.R. and A.R; writing; original concept preparation, S.R. and A.R; writing; revision and editing, A.R. and J.A.V.; supervision, J.A.V. and A.R.; project administration, J.A.V. and A.R.; funding sources, J.A.V. and A.R. All authors read the published version of the manuscript and agreed to the publication thereof.

Dedicated to Prof. Roger Alberto (University of Zürich) on his retirement.

References

Advani, A., Prinz, D., Smurra, A., et al., 2021, What is the case for carbon taxes in developing countries? *IFS*. https://doi.org/10.1920/co.ifs.2024.0383. Accessed 11/15/2021

Alder, C., Hayler, J., Henderson, R., et al., 2016, Updating and further expanding GSK's solvent sustainability guide, *Green Chem* 13, 3879-3890. https://doi.org/10.1039/C6GC00611F.

Arayachukiat, S., Kongtes, C., Barthel, A., et al., 2017, Ascorbic acid as a bifunctional hydrogen bond donor for the synthesis of cyclic carbonates from CO_2 under ambient conditions, *ACS Sustainable Chem Eng* 5, 6392-6397. https://doi.org/10.1021/acssuschemeng.7b01650

Aresta, M., van Eldik, R, 2014, (Eds) Advances in Inorganic Chemistry, CO_2 Chemistry (1st Edition ed.), *Academic Press: London*.

Armarego, W., 2017, Chapter 3 - Purification of Organic Chemicals, *Purification of laboratory chemicals (Eighth Edition)* 95-634. https://doi.org/10.1016/B978-0-12-805457-4.50003-3.

Bar-Even, A., Noor, E., Lewis, N., et al., 2010, Design and analysis of synthetic carbon fixation pathways, *Proc Natl Acad Sci USA* 8889-8894. https://doi.org/10.1073/pnas.0907176107.

Bello Forero, J., Hernández Muñoz, J., Jones Junior, J., et al., 2016, Propylene carbonate in organic synthesis: Exploring its potential as a green solvent, *Curr Org Synth* 13(6), 834-46. https://doi.org/10.2174/1570179413999160211094705.

Berardi, S., Drouet, S., Francàs, L., Gimbert-Suriñach, C., Guttentag, M., Richmond, C., . . . Llobet, A. (2014). Molecular artificial photosynthesis. Chem. Soc. Rev., 7501-7519. https://doi.org/10.1039/C3CS60405E

Berh, A., Naendrup, F., Obst, D., 2002, Platinum-catalysed hydrosilylation of unsaturated fatty acid esters, *Adv Synth Catal* 344(10), 1142-5. https://doi.org/10.1002/1615-4169(200212)344:10<1142::AID-ADSC1142>3.0.CO;2-P.

Bianca, F.B., Dolmella, A., Antonaroli, S., et al., 2002, Five-coordinate complexes of palladium(II) and platinum(II) with α-diimine and 1,5-cyclooctadiene ligands, *J Chem Soc Dalton Trans* 2, 212-217. https://doi.org/10.1039/b106247f.

Blunden, J., Boyer, T., 2021, State of the climate in 2020, *Bull Am Meteorol Soc* 102(8), S1-S475. https://doi.org/10.1175/2021BAMSStateoftheClimate.1.

Bruker., 2021, TopSpin: Version 4.1.3, Bruker Inc.: Madison, Wisconsin, USA, 2021. Madison, Wisconsin, USA: Bruker.

Büttner, H., Steinbauer, J., Wulf, C., et al., 2017, Organocatalyzed synthesis of oleochemical carbonates from CO_2 and renewables, *ChemSusChem* 10(6), 1076-1070. https://doi.org/10.1002/cssc.201601163.

Cauwenbergh, R., Goyal, V., Maiti, R., et al., 2022, Challenges and recent advancements in the transformation of CO_2 into carboxylic acids: straightforward assembly with homogeneous 3d metals, *Chem Soc Rev* 51(22), 9371-423. https://doi.org/10.1039/D1CS00921D.

ClimateActionTracker, 2021, Net zero targets, Available from: https://climateactiontracker.org/methodology/net-zero-targets/. Accessed 11/15/2021.

De Bruin, B., Boerakker, M.B., Donners, J., et al., 1999, Selective oxidation of $[Rh^{I}(cod)]^{+}$ by H_2O_2 and O_2, *Chem Eur J* 5(10), 2921-36. https://doi.org/10.1002/(SICI)1521-3765(19991001)5:10<2921::AID-CHEM2921>3.0.CO;2-1.

Dekker, G., Buijs, A., Elsevier, C., et al., 1992, New neutral and ionic methyl and chloro palladium and platinum complexes containing hemilabile phosphorus-nitrogen ligands. Study of the insertion of carbon monoxide into the metal-methyl bond, *Organometallics* 11(5), 1937-48. https://doi.org/10.1021/om00041a028.

Dolai, M., Saha, U., Biswas, S., et al., 2020, DNA intercalative trinuclear Cu(II) complex with new trans axial nitrato ligation as an efficient catalyst for atmospheric CO_2 fixation to epoxides, *Cryst Eng Comm* 48, 8374-86. https://doi.org/10.1039/D0CE01152E.

Earth.Org., 2021, What countries have a carbon tax? Available from: https://earth.org/what-countries-have-a-carbon-tax/. Accessed 11/15/2021.

Enders, M., Görling, G., Braun, A., et al., 2014, Cytotoxicity and NMR studies of platinum complexes with cyclooctadiene ligands, *Organometallics* 33(15), 4027-34. https://doi.org/10.1021/om500540x.

Fawzy, S., Osman, A., Doran, J., et al., 2020, Strategies for mitigation of climate change: a review, *Environ Chem Lett* 18, 2069-94. https://doi.org/10.1007/s10311-020-01059-w.

Flörke, U., Ortmann, U., Haupt, H., 1992, Rhodium(I)-cyclo¬octadiene (cod) complexes with the N-donor ligands 1,8-di¬azabi¬cyclo[5.4.0]undec-7-ene (dbu) and 1,5-di¬azabi-cyclo[4.3.0]non-5-ene (dbn), *Acta Cryst* 48, 1663-5. https://doi.org/10.1107/S0108270191015111.

Guil-López, R., Mota, N., Llorente, J., et al., 2019, Methanol synthesis from CO_2: A review of the latest developments in heterogeneous catalysis, *Materials* 12(23), 3902. https://doi.org/10.3390/ma12233902.

Guo, L., Lamb, K., North, M., 2021, Recent developments in organocatalysed transformations of epoxides and carbon dioxide into cyclic carbonates, *Green Chem* 23(1), 77-118. https://doi.org/10.1039/D0GC03465G.

Heldebrant, D., Jessop, P., Thomas, C., et al., 2005, The reaction of 1,8-Diazabicyclo[5.4.0]undec-7-ene (DBU) with carbon dioxide, *J Org Chem* 70(13), 5335-8. https://doi.org/10.1021/jo0503759.

Hill, T., 2011, PhD Thesis Diolefin Complexes of Transition Metals as "Venus Fly-Trap" Templates. Bloemfontein, South Africa: University of the Free State.

Hill, T., Roodt, A., 2018, Solid-state and computational study of "Venus fly-trap" geometric parameters for 1,5-Cyclooctadiene in Pd(II) and Pt(II) β-Enaminonato complexes, *Z Anorg Allg Chem* 644(14), 763-774. https://doi.org/10.1002/zaac.201800097.

Hill, T., Roodt, A., Steyl, S., 2013, Probing the 'Venus fly-trap' parameters of cyclo-octadiene in selected beta-diketonato complexes of platinum(II) and the nickel-triad from a spectroscopic, X-ray crystallographic and DFT study, *Polyhedron* 50(1), 82-9. https://doi.org/10.1016/j.poly.2012.10.043.

Jessop, P., 2011, Searching for green solvents, *Green Chem* 6, 1391-8. https://doi.org/10.1039/c0gc00797h.

Ren, M., Jiang, L., Jones, T., Zou, F. (2022). Catalytic Hydrogenation of CO_2 to Methanol: A Review. Catalysts, 12, 403. https://doi.org/10.3390/catal12040403.

Khoshro, H., Zare, H., Namazian, M., et al., 2013, Synthesis of cyclic carbonates through cycloaddition of electrocatalytic activated CO_2 to epoxides under mild conditions, *Electrochim Acta* 113, 263-8. https://doi.org/10.1016/j.electacta.2013.09.080.

Kim, Y., Tanaka, K., Matsuoka, S., 2020, Environmental and economic effectiveness of the Kyoto Protocol, *Plos ONE* e0236299. https://doi.org/10.1371/journal.pone.0236299.

Klein, A., Lepski, R., 2009, 2,2 '-Bipyridine as both bridging and terminal ligand in the binuclear palladium complex $[(\mu\text{-}\eta^1,\eta^1\text{-bpy})\{Pd(Me)(bpy)\}_2](SbF_6)_2$ - Structure and spectroscopic properties, *Z Anorg Allg Chem* 635(6-7), 878-84. https://doi.org/10.1002/zaac.200801398.

Klein, A., Klinkhammer, K., Scheiring, T., 1999, Cyclooctadienemethylplatinum complexes: synthesis, reactivity, molecular structure and spectroscopic properties of the organometallic hydroxoplatinum(II) complex [(COD) PtMe(OH)], *J Organomet Chem* 592(1), 128-135. https://doi.org/10.1016/S0022-328X(99)00500-8.

Klein, A., Neugebauer, M., Krest, A., et al., 2015, Five coordinate platinum(II) in $[Pt(bpy)(cod)(Me)][SbF_6]$: A structural and spectroscopic study, *Inorganics*, 3(2), 118-38. https://doi.org/10.3390/inorganics3020118.

Krieg, B., Taghavi, S., Amidon, G., et al, 2015, In vivo predictive dissolution: Comparing the effect of bicarbonate and phosphate buffer on the dissolution of weak acids and weak bases, *J Pharm Sci* 104(9), 2894-904. https://doi.org/10.1002/jps.24460.

Kuehnel, M., Orchard, K., Dalle, K., et al., 2017, Selective photocatalytic CO_2 reduction in water through anchoring of a molecular Ni catalyst on CdS nanocrystals, *J Am Chem Soc* 139(21), 7217-23. https://doi.org/10.1021/jacs.7b00369.

Lamb, K., 2019, Ch. 15. Catalysts for the conversion of CO2 to cyclic and polycarbonates. In M. North, & P. Styring (Eds.), Volume 2 Transformations (pp. 283-302). Boston, Berlin: De Gruyter. https://doi.org/10.1515/9783110665147-015.

Lamb, W., Wiedmann, T., Pongratz, J., et al., 2021, A review of trends and drivers of greenhouse gas emissions by sector from 1990 to 2018, *Environ Res Lett* 16, 073005. https://doi.org/10.1088/1748-9326/abee4e

Le Quéré, C., Peters, G., Friedlingstein, P., et al., 2021, Fossil CO_2 emissions in the post-COVID-19 era, *Nat Clim Chan* 11, 197-199. https://doi.org/10.1038/s41558-021-01001-0.

Lee, T.-Y., Lin, Y.-J., Chang, Z.-Y., et al., 2017, Nickel-catalyzed coupling of carbon dioxide with cyclohexene oxide by well-characterized Bis(N-Heterocyclic Carbene) carbazolide complexes, *Organometallics* 36(2), 291-7. https://doi.org/10.1021/acs.organomet.6b00756.

Leipoldt, J., Van Eldik, R., Basson, S., et al., 1983, Kinetics and mechanism of the reaction between trans-dioxotetracyanotungstate (IV) and azide in aqueous solution, *Inorganic Chemistry*, 25(26), 4639-4642. https://doi.org/10.1021/ic00246a010.

Lenden, P., Ylioja, P., González-Rodríguez, C., et al., 2011, Replacing dichloroethane as a solvent for rhodium-catalysed intermolecular alkyne hydroacylation reactions: the utility of propylene carbonate, *Green Chem* 8, 1980-2. https://doi.org/10.1039/c1gc15293a.

Lepski, R., Lüning, A., Stirnat, K., et al., 2014, Unexpected formation of [(Me2-Xyl-DAB)Pd(η3–6-methyloct-2-en-1-id)][SbF6] (Me2-Xyl-DAB= 2,3-dimethyl-1,4-bis(2,6-dimethylphenyl)-diazabuta-1,3-diene), *J Organomet Chem* 751, 821-5. https://doi.org/10.1016/j.jorganchem.2013.07.071.

Martin, C., Florani, G., Kleij, A., 2015, Recent advances in the catalytic preparation of cyclic organic carbonates, *ACS Catal* 5(2), 1353-70. https://doi.org/10.1021/cs5018997.

Masson-Delmotte, V., Zhai, P., Pirani, A., et al., 2021, IPCC, 2021: Climate Change 2021: The Physical Science Basis. (Contribution of Working Group I to the 6th Assessment Report of the Intergovernmental Panel on Climate Change) 2391pp. Cambridge (UK); New York (USA): Cambridge Univerity Press.

Moghimi, A., Khavassi, H., Dashtestani, F., et al., 2011, A ternary tetracoordinated PdII complex with metformin and dipicolinate: Synthesis, characterization and crystal structure, *J Mol Struct* 996, 38-41. https://doi.org/10.1016/j.molstruc.2011.03.061.

Nakada, A., Koike, K., Maeda, K., et al., 2015, Highly efficient visible-light-driven CO_2 reduction to CO using a Ru(II)-Re(I) supramolecular photocatalyst in an aqueous solution, *Green Chem* 1, 139-43. https://doi.org/10.1039/C5GC01720C.

NOAA-Global-Monitoring-Laboratory-US-Department-of-Commerce. (2021). The NOAA Annual Greenhouse Gas Index (AGGI), 2021. Retrieved from https://gml.noaa.gov/aggi/aggi.html. Accessed 11/12/2021

North, M., Styring, P.E., 2019, Carbon dioxide utilisation transformations (Volume 2 ed.). Boston: De Gruyter.

O'Meara, S., 2020, China's plan to cut coal and boost green growth, *Nature* S1-S3. https://doi.org/10.1038/d41586-020-02464-5.

OriginLab, 2021, OriginPro: Version 2021b. Northampton, Masechusetts, USA: OriginLab Corporation.

Paddock, R., Nguyen, S., 2004, Chiral (salen)Co(III) catalyst for the synthesis of cyclic carbonates, *Chem Commun* 14, 1622-3. https://doi.org/10.1039/b401543f.

Panepinto, D., Riggio, V., Zanetti, M., 2021, Analysis of the emergent climate change mitigation technologies, *Int J Environ Res Public Health* 18(13) 6767. https://doi.org/10.3390/ijerph18136767.

Pescarmona, P., 2021, Cyclic carbonates synthesised from CO2: Applications, challenges and recent research trends, *Current Opinion in Green and Sustainable Chemistry* 29, 100457. https://doi.org/10.1016/j.cogsc.2021.100457.

Pescarmona, P., Tahermehr, M., 2012, Challenges in the catalytic synthesis of cyclic and polymeric carbonates from epoxides and CO_2, *Catal Sci Technol* 2, 2169-87. https://doi.org/10.1039/c2cy20365k.

Pradhan, S., Das, S., 2023, Recent advances on the carboxylations of C(sp^3)-H bonds using CO_2 as the carbon source, *Synlett* 34(12), 1327-42. https://doi.org/10.1055/a-2012-317.

Purcell, W., Roodt, A., Basson, S., et al., 1989, Kinetic study of the reaction between trans-tetracyanodioxorhenate(V) and thiocyanate ions, *Transition Metal Chemistry* 14, 224-6. https://doi.org/10.1007/BF01043801.

Ramidi, P., Gerasimchuk, N., Gartia, Y., et al., 2013, Synthesis and characterization of Co(III) amidoamine complexes: influence of substituents of the ligand on catalytic cyclic carbonate synthesis from epoxide and carbon dioxide, *Dalton Trans* 36, 13151-60. https://doi.org/10.1039/c3dt51352a.

Redgard, S., 2019, MSc Dissertation: Nucleophile Assisted Carbon Dioxide Fixation for a Cleaner Environment. Blloemfontein, South Africa: University of the Free State.

Redgard, S., 2021, PhD Thesis: Solid State and Kinetic Study of Diolefin Complexes of Platinum Group Elements. Bloemfontein, South Africa.: University of the Free State.

Ritchie, H., Roser, M., 2021, CO_2 and greenhouse gas emissions. Available form: https://ourworldindata.org/co2-emissions. Accessed 11/13/2021.

Roodt, A., Venter, J., Redgard, S., 2022, NMR, kinetic mechanistic and SC-XRD study of carbon dioxide capturing model molecular materials, *Acta Crystallographica* 78, a582-a582. https://doi.org/10.1107/S2053273322091847.

SA-Akademie-vir-Wetenskap-en-Kuns, 2023, Suid-Afrikaanse Akademie vir Wetenskap and Kuns. Available from: https://assets-global.website-files.com/638efa1bbea3b03765963904/6458c9622d121cb02bc5e208_2_SAAWK_Nuusbrief%20April%202023_Akademiepryse.pdf. Accessed October 01, 2023.

Schäffner, B., Andrushko, V., Holz, J., et al., 2008, Rh-catalyzed asymmetric hydrogenations of unsaturated lactate precursors in propylene carbonate, *ChemSusChem* 1(11), 934-40. https://doi.org/10.1002/cssc.200800157.

Schäffner, B., Holz, J., Verevkin, S., et al., 2008, Rhodium-catalysed asymmetric hydrogenation with self-assembling catalysts in propylene carbonate, *Tetrahedron Lett* 49(5), 768-71. https://doi.org/10.1016/j.tetlet.2007.11.199.

Scheffen, M., Marchal, D., Beneyton, T., et al., 2021, A new-to-nature carboxylation module to improve natural and synthetic CO^2 fixation, *Nat Catal* 4, 105-15. https://doi.org/10.1038/s41929-020-00557-y.

Schilling, W., Das, S., 2020, Transition metal-free synthesis of carbamates using CO_2 as the carbon source, *ChemSusChem* 13(23), 6246-58. https://doi.org/10.1002/cssc.202002073.

Schlüter, U., Weber, A., 2020, Regulation and evolution of C4 photosynthesis, *Ann Rev Plant Biol* 71, 183-215. https://doi.org/10.1146/annurev-arplant-042916-040915.

Seipp, C., Williams, N., Kidder, M., et al., 2017, CO_2 capture from ambient air by crystallization with a guanidine sorbent, *Angew Chem Int Ed* 56(4), 1042-5. https://doi.org/10.1002/anie.201610916.

Smit, J., Purcell, W., Roodt, A., et al., 1993, Kinetics of the substitution reaction between aquaoxotetracyanomolybdate (IV) and cyanide/hydrogen cyanide, *Polyhedron* 12, 2271-7. https://doi.org/10.1016/S0277-5387(00)88267-4.

Sopeña, S., Cozzolino, M., Maquilón, C., et al., 2018, Organocatalyzed domino [3+2] Cycloaddition/Payne-Type rearrangement using carbon dioxide and epoxy alcohols, *Angew Chem Int Ed* 57(35), 11203-7. https://doi.org/10.1002/anie.201803967.

Štěpnička, P., Císařová, I., 1996, Crystal structure of Dibromo(η4-1,5-cyclooctadiene) palladium(II), *Collect Czech Chem Commun* 61(9), 1335-41. https://doi.org/10.1135/cccc19961335.

Trudeau, D., Edlich-Muth, C., Zarzycki, J., et al., 2018, Design and in vitro realization of carbon-conserving photorespiration, *Proc Natl Acad Sci USA* 115(49), E11455-64. https://doi.org/10.1073/pnas.1812605115.

Van der Westhuizen, H., Meijboom, R., Schutte, M., et al., 2010, Mechanism for the formation of substituted manganese(V) cyanidonitrido complexes: crystallographic and kinetic study of the substitution reactions of trans-$[MnN(H_2O)(CN)_4]^{2-}$ with monodentate ligands, *Inorganic Chemistry* 49(20), 9599-608. https://doi.org/10.1021/ic101274q.

Vermaak, V., Vosloo, H., Swarts, A., 2024, The development and application of homogeneous nickel catalysts for transfer hydrogenation and related reactions, *Coord Chem Rev* 507, 215716. https://doi.org/10.1016/j.ccr.2024.215716.

Wang, Z., Bu, Z., Cao, T., et al., 2012, A novel and recyclable catalytic system for propylene carbonate synthesis from propylene oxide and CO_2, *Polyhedron* 32(1), 86-9. https://doi.org/10.1016/j.poly.2011.07.002.

Watt, F., Sieland, B., Dickmann, N., Schoch, R., et al., 2021, Coupling of CO_2 and epoxides catalysed by novel N-fused mesoionic carbene complexes of Nickel(II), *Dalton Trans* 50, 17361-71. https://doi.org/10.1039/D1DT03311E.

Weber, A., Bar-Even, A., 2019, Update: Improving the efficiency of photosynthetic carbon reactions, *Plant Physiol* 803-812. https://doi.org/10.1104/pp.18.01521.

Wu, Y., Jiang, Z., Lu, X., Liang, Y., et al., 2019, Domino electroreduction of CO_2 to methanol on a molecular catalyst, *Nature* 575, 639-42. https://doi.org/10.1038/s41586-019-1760-8.

Yingcharoen, P., Kongtes, C., Arayachukiat, S., et al., 2019, Assessing the pKa-dependent activity of hydroxyl hydrogen bond donors in the organocatalyzed cycloaddition of carbon dioxide, *Adv Synth Catal* 361, 366-3. https://doi.org/10.1002/adsc.201801093.

Yoshida, Y., Aoyagi, N., Endo, T., 2018, Selective formation of a zwitterion adduct and bicarbonate salt in the efficient CO_2 fixation by N-benzyl cyclic guanidine under dry and wet conditions, *Beilstein J Org Chem* 14, 2204-11. https://doi.org/10.3762/bjoc.14.194.